REPORT NO. DOT-TSC-NASA-71-12

OPTICAL COMMUNICATIONS AND DETECTION SYSTEMS

R. E. BUCK, R. GAGNON, L. M. JORDAN,
S. KARP, E. T. LEONARD, S. J. MORIN
TRANSPORTATION SYSTEMS CENTER
55 BROADWAY
CAMBRIDGE, MA. 02142

AUGUST 1971
TECHNICAL REPORT

Prepared for
NATIONAL AERONAUTICS AND SPACE ADMINISTRATION
WASHINGTON, D. C. 20546

1. Report No.	2. Government Accession No.	3. Recipient's Catalog No.
DOT-TSC-NASA-71-12		

4. Title and Subtitle	5. Report Date
Optical Communications & Detection System	August 1971
	6. Performing Organization Code: TEC
7. Author(s): R.E. Buck, R. Gagnon, L.M. Jordan, S. Karp	8. Performing Organization Report No.: DOT-TSC-NASA-71
9. Performing Organization Name and Address: U.S. Dept. of Transportation, Transportation Systems Center, Cambridge, MA 02124	10. Work Unit No.: NA03-1
	11. Contract or Grant No.
	13. Type of Report and Period Covered: Final Report July 1, 1970 - June 30, 1971
12. Sponsoring Agency Name and Address: National Aeronautics and Space Administration, Washington, DC 20546	14. Sponsoring Agency Code

15. Supplementary Notes

Authors cont. E.T. Leonard, and S.J. Morin

16. Abstract The two milestones of the program (1) development of a high quantum efficiency 1.06 micron photoemissive surface and (2) narrow pulse propagation in the earth's atmosphere at 0.63 microns were completed.

Item 1 was completed in a contract award.

Item 2 was complete to the extent permitted by the weather conditions in that only two foggy days were encountered during the three month period.

The clear air measurements indicated that: pulse broadening in the atmosphere is less than 20 picoseconds or a coherence bandwidth in excess of 50 GHz; aperture averaging appears to progress with the square of the collector diameter for large diameters; statistics of aperture averaged signals remain log normal.

The measurements from one foggy day indicate: no pulse broadening was observed in fogs with ¼ mile visibility although a 20 dB loss was encountered; no return from multiple scattering could be observed to a 4 degree field of view with a 20 dB dynamic range in the detector; no Doppler broadening greater than 1 KHz was observed with optical thickness as high as 4.

17. Key Words	18. Distribution Statement
Laser pulse broadening Earths Atmosphere 1.06 Micron Scintillation Fog Clear Air	Availability is Unlimited. Document may be Released To the National Technical Information Service, Springfield, Virginia 22151, for Sale to the Public.

19. Security Classif. (of this report)	20. Security Classif. (of this page)	21. No. of Pages	22. Price
Unclassified	Unclassified	101	

PREFACE

The authors are indebted to Mr. Henry Anderton and Mr. John Meson of the NASA Headquarters and to Dr. Gene G. Manella, Mr. L. W. Roberts, Mr. C. M. Veronda, and Dr. R. D. Kodis at the Transportation Systems Center for their support and encouragement of this work. The authors would like to acknowledge Mr. Valente for efficient procurement of vital parts.

TABLE OF CONTENTS

LIST OF ILLUSTRATIONS

LIST OF ILLUSTRATIONS (Cont)

1. OVERVIEW

1.1 SUMMARY

The two milestones of the program, 1. development of a high quantum efficiency 1.06 micron photoemissive surface; 2. narrow pulse propagation measurements, were completed. Item 1. resulted in a contract award to Varian Associates, the technical direction of which was transferred to Goddard Space Flight Center. Item 2. was completed to the extent permitted by weather conditions, in that only two foggy days were encountered during the three month measurement period. The clear air measurements indicate that:

1. Pulse broadening in the atmosphere is less than 20 picoseconds or a coherence bandwidth in excess of 50 GHz.
2. Aperture averaging appears to progress with the square of the collector diameter for large diameters.
3. Statistics of aperture averaged signals remain log normal.

Measurements from the one foggy day indicate:

1. No pulse broadening was observed in fogs with 1/4 mile visibility ,although a 20 dB loss was encountered.
2. No return from multiple scattering could be observed to a 4° field of view with a 20 dB dynamic range in the detector.
3. No doppler broadening greater than 1 kHz was observed with optical thicknesses as high as four.

1.2 BRIEF TECHNICAL DISCUSSION

This work was started at ERC in 1968 as an R & D experimental program that anticipated future problem areas in optical communications. It was also necessary that this program be complementary to other NASA programs in this area.

It was already clear at that time that narrow pulse mode-locked lasers would be valuable sources for optical communications (Karp, O'Neil, and Gagliardi, 1970; Karp and Clark, 1970; Clark and Karp, 1970). In fact, work had already progressed in trying to measure the coherence bandwidth of the atmosphere, but was limited to about 500 MHz (it has since been recognized that the coherence bandwidth is on the order of 100 GHz, Brookner, 1970). It was also clear that one of the limiting factors in optical communications was the inability

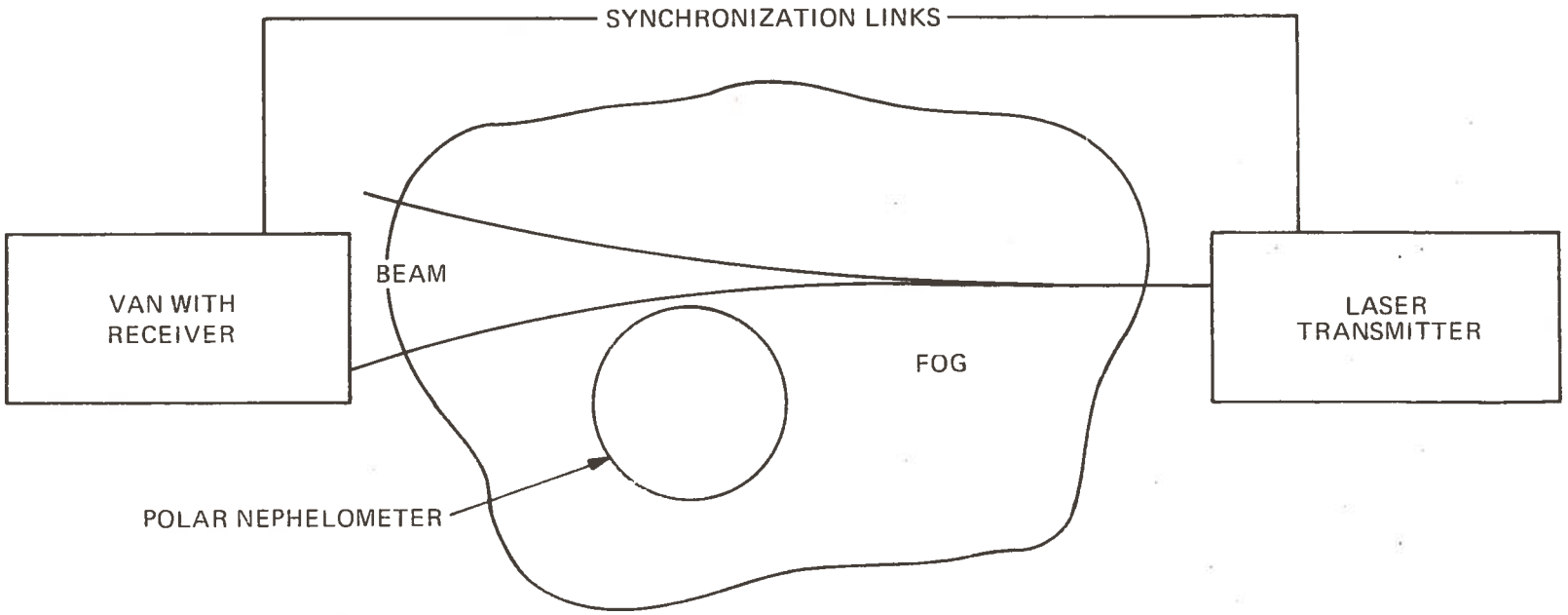

Figure 1. Schematic Diagram of the Experiment.

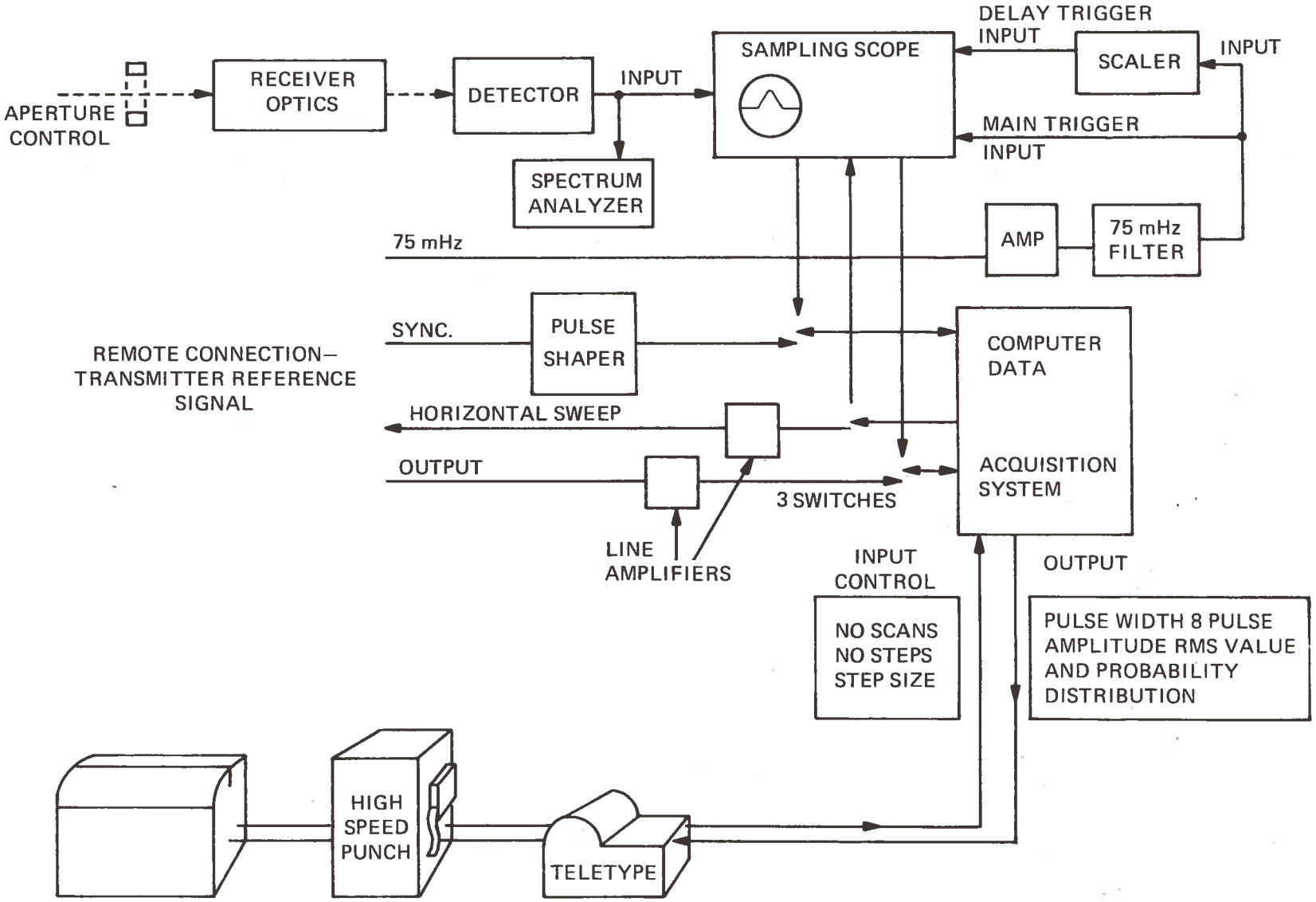

Figure 3. Schematic Diagram of the Receiver System.

minimum of broadening was expected in clear weather. A computer was purchased to perform on-line signal processing. All computer programs relevant to the experiment were completed and checked out in the laboratory. A simple diagram of the sampled construction of the waveform is shown in Figure 5. Results showed a measurement resolution of better than 10 picoseconds of pulse broadening in the laboratory, but the best that could be obtained in the field was 25 picoseconds.

1.4 MEASUREMENTS IN CLEAR WEATHER

We refer to this portion as the "clear weather" portion where we are considering extremely large coherence bandwidths. These large bandwidths occur generally on clear days but have been shown to exist as well on line-of-sight paths in haze and fog by Kerr at Oregon State.

Since the atmosphere has fading components of no more than a few hundred cycles, it is possible to combine sampling techniques and mode-locked lasers to make accurate pulse broadening measurements. For example, a sampling scope was procured which has a 28 picosecond gate and operates at about 80 kHz. Thus, in 5 milliseconds 400 samples could be taken with the atmoshpere frozen. The output of a model 125 Spectra Physics mode-locked laser consists of a train of one nanosecond pulses spaced 13 nanoseconds apart. An SEL810B computer was selected because it could do the required processing between samples which were 12.5 μsec apart. This processing merely consisted of keeping a running sum of each sample associated with a particular portion of the trace. At the conclusion of the experiment there would exist 400 numbers representing the total accumulation of sample points. These 400 points are then used to calculate the pulse broadening. It was felt initially that using a stored replica of the unbroadened pulse, the impulse response of the channel could be extracted by deconvolution. This, however, proved futile and an alternate calculation was made (the Fast Fourier Transform is still a viable alternative for deconvolution). The calculations made were simple and accurate. The rms pulse broadening, Δi, was defined as:

$$\Delta i = \left[\frac{\sum_{i=1}^{400} (i - \bar{i})^2 y_i}{\sum_{i=1}^{400} y_i} \right]^{1/2}$$

where

$$\bar{i} = \sum_{i=1}^{400} iy_1 \Big/ \sum_{i=1}^{400} y_i$$

y_1 is the amplitude of the i^{th} sample, and i is the sample number. The programs for computer control of the whole system are complete. The following tests were run:

1. The undistorted pulse width was measured by this technique on an hourly and daily basis for a period of one to two weeks. The rms spread of these measurements was about one-half a sample and an estimated 6 to 9 picoseconds.
2. A split beam Michelson interferometer arrangement was set up with one mirror mounted on a micrometer drive. The rms pulse width was measured as the time displacement between pulses went through zero. Using the micrometer as a guide, it was again estimated that the rms spread was about 6 to 9 picoseconds.

The following conclusions were drawn: On a static basis the repeatability and resolution of the system appear limited by the jitter in the scope and the 4 nanosecond scope scale used. On a dynamic basis it appears that the measurement can resolve the 6 to 9 picosecond broadening of the pulse.

Although the rms pulse measurement has quantitative significance with regard to the coherence bandwidth, it was difficult to make the measurement under the highest resolution condition, i.e., when only a part of the pulse was displayed on the scope. Therefore, a second measurement which measured the time difference between the 3dB points of the pulse was programmed to run concurrent. This gave another measure for

2. DETAILED EXPERIMENT DESIGN CONSIDERATIONS

2.1 INTRODUCTION

The optical communication experiment was conducted at Otis A.F.B., Falmouth, Massachusetts, where there is a high incidence of foggy weather. Also Otis A.F.B. has available a large unobstructed level area that was especially suitable for the experiment. The experimental design consisted of a laser transmitter and receiver (See Figures 1, 2, 3, 4). The transmitter was a mode-locked He-Ne laser that provided an optical pulse with a duration of about one nanosecond. This pulse duration represents approximately the current limitation on the response time of a photomultiplier. The laser output was monitored for pulse width and amplitude variations that could occur due to component aging. The receiver, which was located approximately 0.5 miles from the laser transmitter, consisted of a lense collecting system, a fast response time detector, a wide bandwidth sampling oscilloscope, and an on-line computer. The lense collecting system had an adjustable field of view and aperture to allow tests to be conducted relating detector area and acceptance solid angle to channel impulse transmission response under a range of varying fog and haze conditions. The output of the detector was displayed on a wideband sampling oscilloscope. An on-line computer controlled the sampling scope and processed the detected laser pulse, computing pulse width and amplitude distributions. Volume scattering functions for the ambient media were measured by a polar nephelometer to support theoretical analysis and interpretations.

2.2 FIELD SITE

2.2.1 LOCATION

A survey was conducted in the Boston, Massachusetts area for the optical communication experimental field site. After looking at several possible sites, Otis AFB was selected. The Otis AFB site offered high occurrence of fog, a large unobstructed flat area conducive to homogenous fogs, access to the base weather station, and the facilities and security of the military base.

2.2.2 FIELD SITE PREPARATION

After the Otis AFB Civil Engineers were contacted and an acceptable site location agreed upon, field site preparation started. This entailed the installation of concrete mounting pads for the transmitter and receiver azimuth-elevation tables,

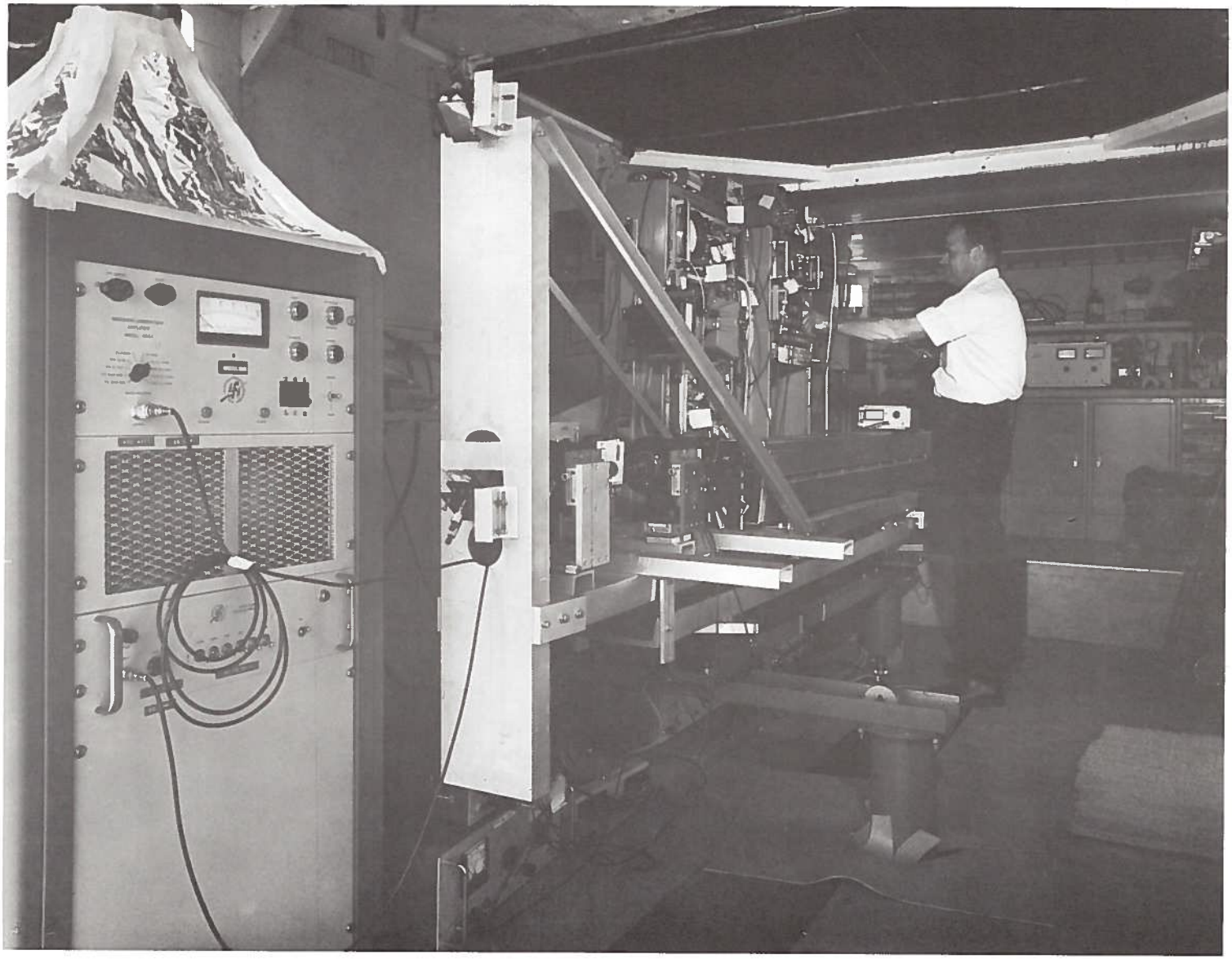

Figure 6. Photograph of the Transmitter Equipment

locking was discarded. A second attempt at mode-locking was made using a frequency synthesizer set at the mode-locking frequency of the laser. The synthesizer drove a piezo electric mirror located at one end of the laser cavity. Long term stability difficulties again occurred caused by the slow drifting of the laser mode-lock frequency away from the synthesizer frequency. Although this mode-locking system was stable for approximate 15-minute intervals it was also discarded. Finally a feedback mode-lock system was purchased from Spectra Physics, the Spectra Physics 360 mode-locker. This system was not available when initial mode-locking techniques were tried.

Being a feedback system which followed the laser cavity temperature drifts, this mode-locker was stable. The Spectra Physics model 125 mode-locked laser output was a train of approximately one nanosecond width pulses spaced approximately 13.2 nanoseconds apart. The output power is approximately 50 milliwatts average and 660 milliwatts peak.

The laser 2 mm diameter beam was expanded to 5 cm by a Tropel model 280-50 collimator to reduce beam divergence. By using this collimator a spot size of 8 inches in diameter could be obtained at the receiver trailer located approximately 1/2 mile away.

2.3.3 OPTICAL GATING SYSTEM

Under heavy fog conditions the received mode-locked laser pulses could possibly be broadened to widths greater than 20 nanoseconds. With the mode-locked laser pulses separated by only 13.2 nanoseconds, pulse broadening under heavy fog conditions would cause overlapping of the laser pulses and pulse width measurements would therefore be impossible.

To overcome these problems an optical gating system was designed to gate through one out of every 1000 laser pulses, increasing the pulse separation distance to 13.2 microseconds, a 75 kHz repetition rate.

It should be noted that the receiver system utilizes a sampling technique that operates at a maximum sampling rate of 100 kHz. Therefore the 75 kHz repetition rate of the gated laser pulse train will not appreciably slow down the data acquisition time required to complete a measurement.

The gating system consists of a scaler, a pockel cell driver, and a pockel cell optical modulator. The 75 MHz electrical signal is sampled from the mode-locked laser feedback amplifier. This 75 MHz signal is scaled down by a factor of 1000 to 75 kHz. The 75 kHz signal drives a pulse generator.

put waveform is reconstructed sample by sample by a Hewlett-Packard sampling oscilloscope. Each of these samples, taken at an approximate 100 kHz repetition rate, is transmitted via a line driver on a coaxial cable to the SEL 810B computer at the receiver trailer, a distance of 1/2 mile. The computer processes the received samples and computes the pulse width and amplitude distribution of the laser wave form. Further description of the sampling scope data acquisition system is described in the receiver system section of this report.

2.4 RECEIVER SYSTEM

2.4.1 GENERAL DESCRIPTION

The receiver consists of a collecting optics, a detector, a sampling oscilloscope and an SEL 810B computer. See Figures 3 and 8. The collecting optics has adjustable aperture and field of view to allow tests to be conducted relating detector area and acceptance solid angle to channel impulse transmission response under a range of varying fog and haze conditions. The collected laser beam is focused on a fast response detector. The detector output wave form is reconstructed sample by sample by a sampling oscilloscope. An SEL 810B computer processes the samples taken by the oscilloscope and calculates the received mode-locked laser pulse width and amplitude probability distribution.

2.4.2 RECEIVER SYSTEM OPTICS

Two sets of receiver optics were used in the Otis field tests. The first was a 12 inch diameter Cassegrain telescope. See Figure 9. A set of aperture stops ranging from 30 cm diameter to 0.5 cm diameter, could be mounted on the front of the Cassegrain.

These stops were used in clear air aperture averaging studies. The Cassegrain telescope had only a 0.4° field of view, which degraded from its usefulness in optical pulse-broadening measurements of multiple scattering in fogs. To increase the usefulness of the Cassegrain telescope in these fog measurements, the complete optical collecting and detecting system could be readily positioned up to 20° off the laser axis by adjusting the azimuth elevation table.

A second optical collecting system was built with a variable field of view from 0.125 to 3.8° for the fog pulse-broadening measurements.

The objective lens on this system was a 27 inch by 17 inch Fresnel lens with a 29 inch focal distance. See Figure 10.

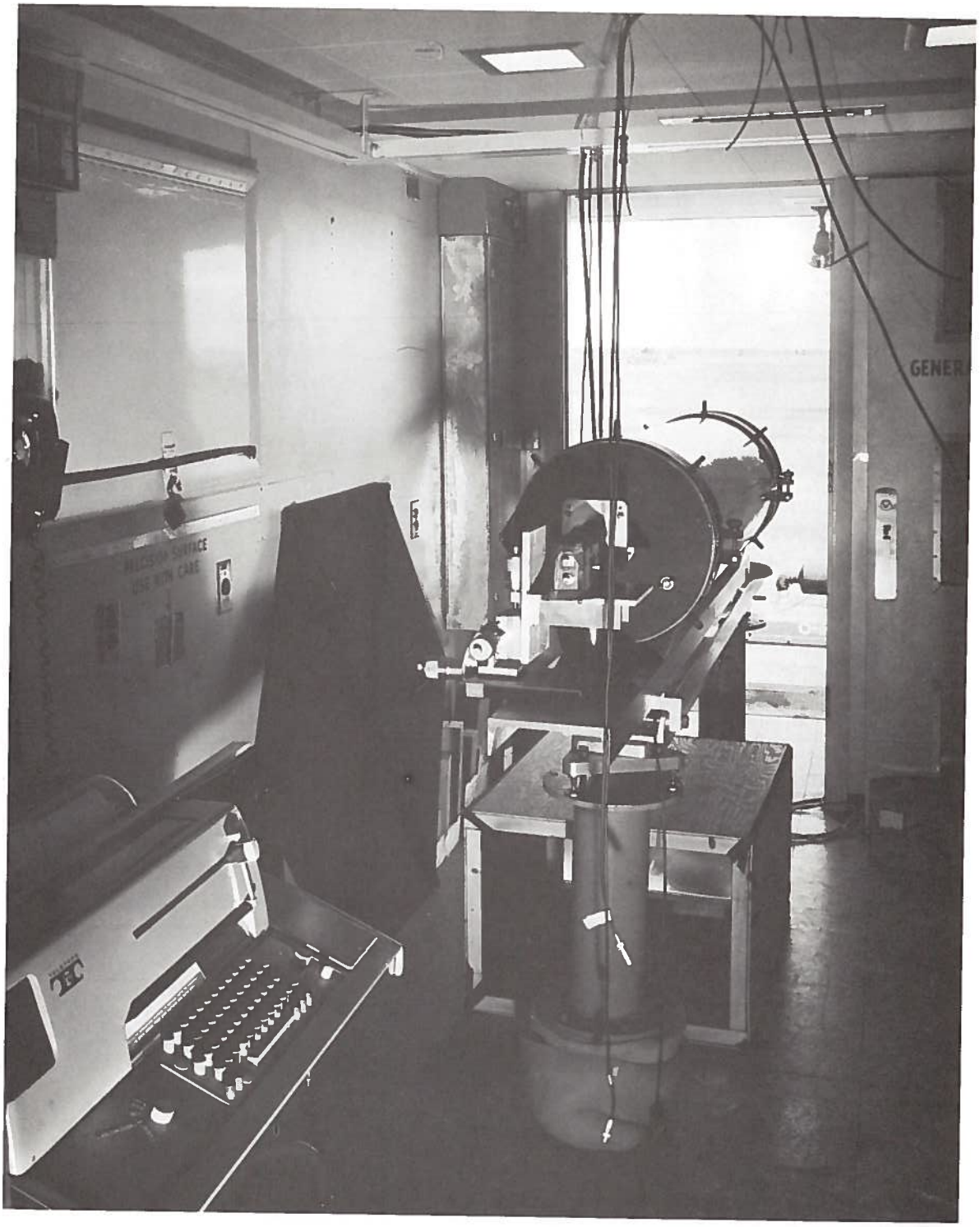

Figure 9. Photograph of the 12 Inch Diameter Cassegra in Telescope.

A semicircle mask was placed in the image plane of the lens system to eliminate all multiple scattering below the laser beam axis, avoiding possible ground reflection errors. Another removable image plane stop was added to the lens system to blank out the main laser beam, allowing the option of viewing only the scattered light component of the laser beam in fog.

2.4.3 DETECTORS

Essentially there were two types of detectors used in the laser communication field tests, wide bandwidth, fast rise time photomultipliers for measurements of the picosecond laser pulse broadening in fogs and slower rise time, narrower bandwidth photomultipliers for amplitude probability studies in clear air turbulance.

The photomultipliers tested for use in the pulse broadening measurements were the Ampex XP1210, Sylvania 502 crossed field, and RCA C70045D. These three photomultipliers represent the fastest response tubes presently available.

The RCA C70045D photomultiplier became "gassy" and developed a voltage breakdown across the last dynode stages. Therefore, the C70045D could not be used.

The XP1210 photomultiplier tested had a rise time of 1 nanosecond and a decay time of 3 nanoseconds. Response times were measured from the 10% to 90% of the peak pulse amplitude and were obtained from the wave shape of a single photoelectron event which is an impulse function.

Because the signal attenuation from multiple scattering due to fog is at least 20 dB greater than from the unscattered component of the laser pulse, the time required for the signal to decay below the 10% peak amplitude value is also of interest.

XP1210 had a decay time of approximately 5 nanoseconds at the -20 dB points, therefore could not be used in measuring multiple scattering fog measurements.

The Sylvania 502 crossed field photomultiplier had the fastest response time of all the photomultipliers tested. Its rise and decay time was approximately 0.1 nanoseconds. The crossed field photomultiplier also had a symmetrical wave form; that is, its rise and decay time were the same. From these measurements the crossed field was an obvious choice for the detector to be used in the fog pulse broadening measurements.

There are two disadvantages to the Sylvania crossed field photomultiplier. The first is the low quantum efficiency of

program has the following inputs:

1. Starting and ending point on the sampling scope;
2. Number of scans to be averaged;
3. The point on the waveform to be analyzed for the probability amplitude distribution measurement;
4. Bias location on the waveform displayed on the scope and method bias is calculated--

    a. minimum point on the waveform,
    b. average of a selected number of points on the waveform.

The computer has the following outputs:

1. 3 dB pulse width calculation;
2. Rms pulse width calculation;
3. Amplitude probability distribution of a point chosen on the waveform displayed on the scope;
4. Binary output on high-speed paper tape and on teletype of stored data acquired;
5. Output for an x-y recorder or scope of the average of the scans taken in the data acquisition.

The data acquisition computer is further documented in Section 6.1.

2.5.2 SAMPLING SCOPE TO COMPUTER INTERFACE

Three interconnections between the sampling scope and the computer are required to operate the acquisition program. See Figure 4. Two of these are for signals from the scope to the computer, the scope sync output and the scope "Y" output. The third connection is for a staircase voltage from the computer that drives the scope's horizontal deflection plates.

The basic operation of the interface is as follows. A trigger input to the scope actuates the sampling circuitry for an extremely short time interval and the waveform at that instant is measured and held for approximately 10 microseconds. This signal is amplified and sent from the scope's "Y" output to the computer. At the instant the sampling circuit is actuated, a sync pulse is also sent from the scope to the computer. This sync pulse is the trigger pulse that signals the computer to read the waveform voltage sample at the "Y" output of the scope via an analog-to-digital converter. The computer, after storing the sampled waveform signal in a memory location, outputs a step in the voltage staircase waveform via a digital-to-analog converter. This voltage step moves the cathode ray tube spot horizontally a short distance and

by blocking or unblocking the beam from the displacement mirror in one of the interferometer arms.

Rms pulse width measurements were conducted on the single pulses and on the double pulses with various separation distances. The accuracy of these rms pulse width measurements was limited to ± one sample out of the 400 samples taken horizontally across the 10 cm face of the sampling oscilloscope. Therefore, at a one nanosecond per cm sweep rate, a 25 picosecond accuracy can be obtained.

The sampling oscilloscope time base is only calibrated to a 1% accuracy. Therefore, pulse width measurements taken at different scope sweep rate settings could have a 1% error. Because of this, the sampling oscilloscope was left on the one nanosecond sweep rate position for all pulse width measurements.

Periodic calibrations were made on both the transmitter reference monitor system and the receiver system at the Otis AFB field site. This was accomplished by connecting a pulse generator having a known pulse width to the sampling scopes input and operating the data acquisition program. The computed pulse width and amplitude probability distribution of the pulse generator output was compared to past calibrations for possible system changes. Both the receiver and transmitter monitor systems remained stable throughout the Otis AFB field tests to ± one sample, 25 picoseconds.

2.7 FREQUENCY BROADENING MEASUREMENTS

A Hewlett-Packard 8551 spectrum analyzer was used to measure Doppler broadening of the laser at the receiver. The Sylvania crossed field photomultiplier output was connected directly into the spectrum analyzer and the envelope of the received laser pulse train was displayed in the frequency domain on the spectrum analyzer. The spectrum analyzer has a maximum spectral resolution of 1 kHz and a minimum scan width of 10 kHz/cm.

2.8 LASER RANGE SAFETY

The 0.5 mile (768 m) long laser test range was located on an unused field at Otis AFB, Falmouth, Massachusetts. The laser beam was maintained at a minimum of 10 feet above ground level and approximately parallel to the ground plane. The laser beam was completely terminated at the receiver trailer. The laser was not operated unless test personnel were on the site.

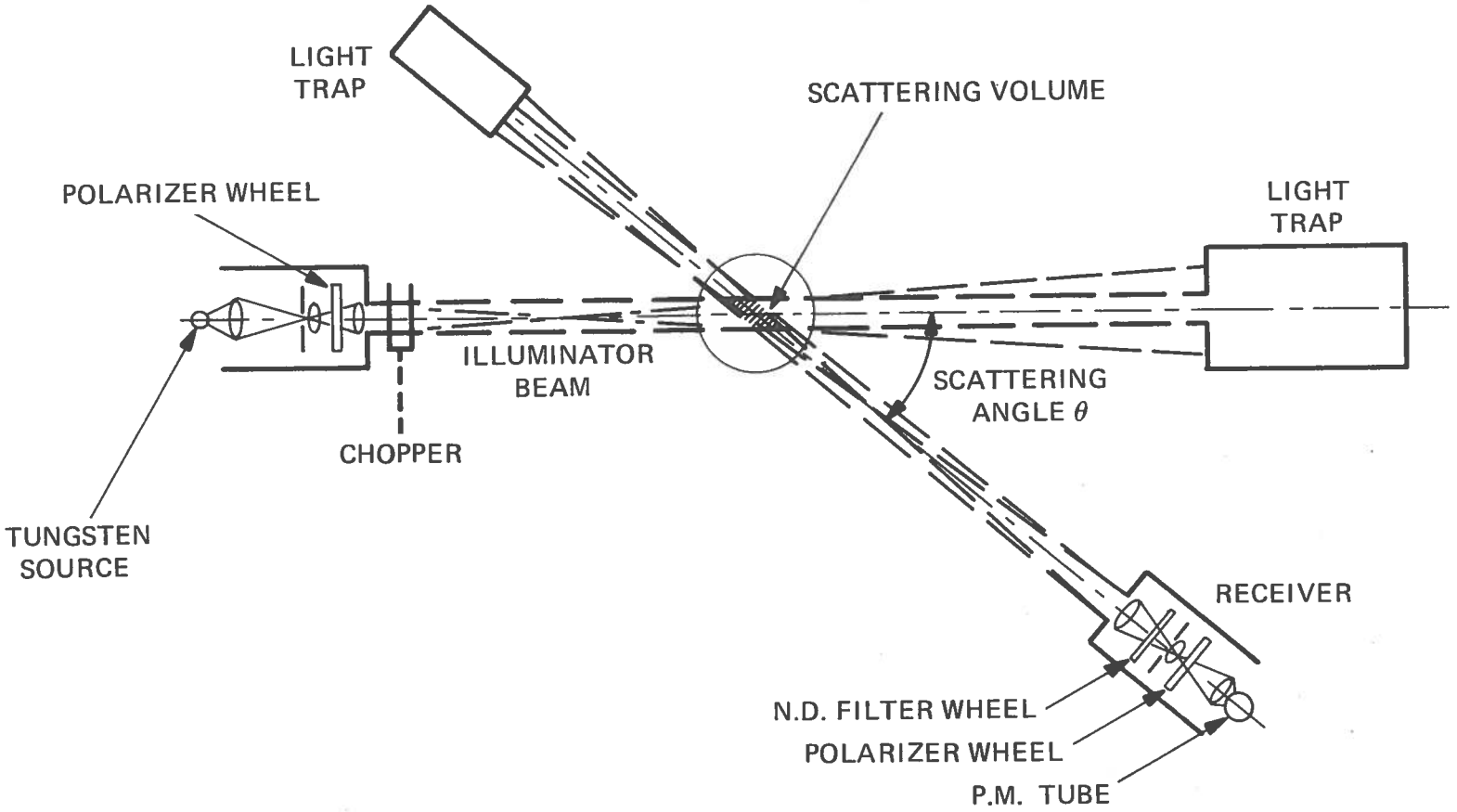

Figure 11. Schematic Diagram of Polar Nephelometer.

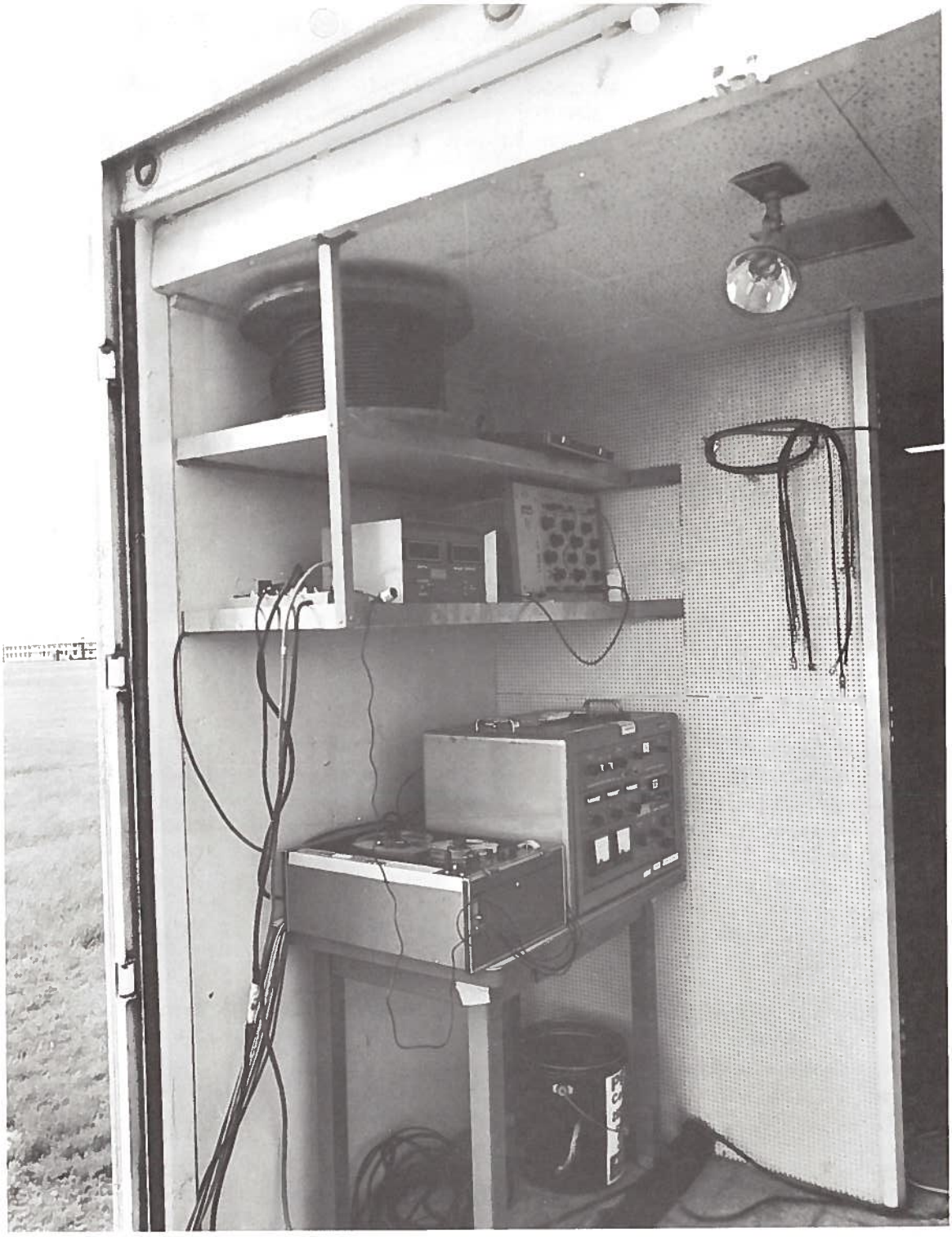

Figure 13. Photograph of the Electronic Instrumentation Associated with the Polar Nephelometer.

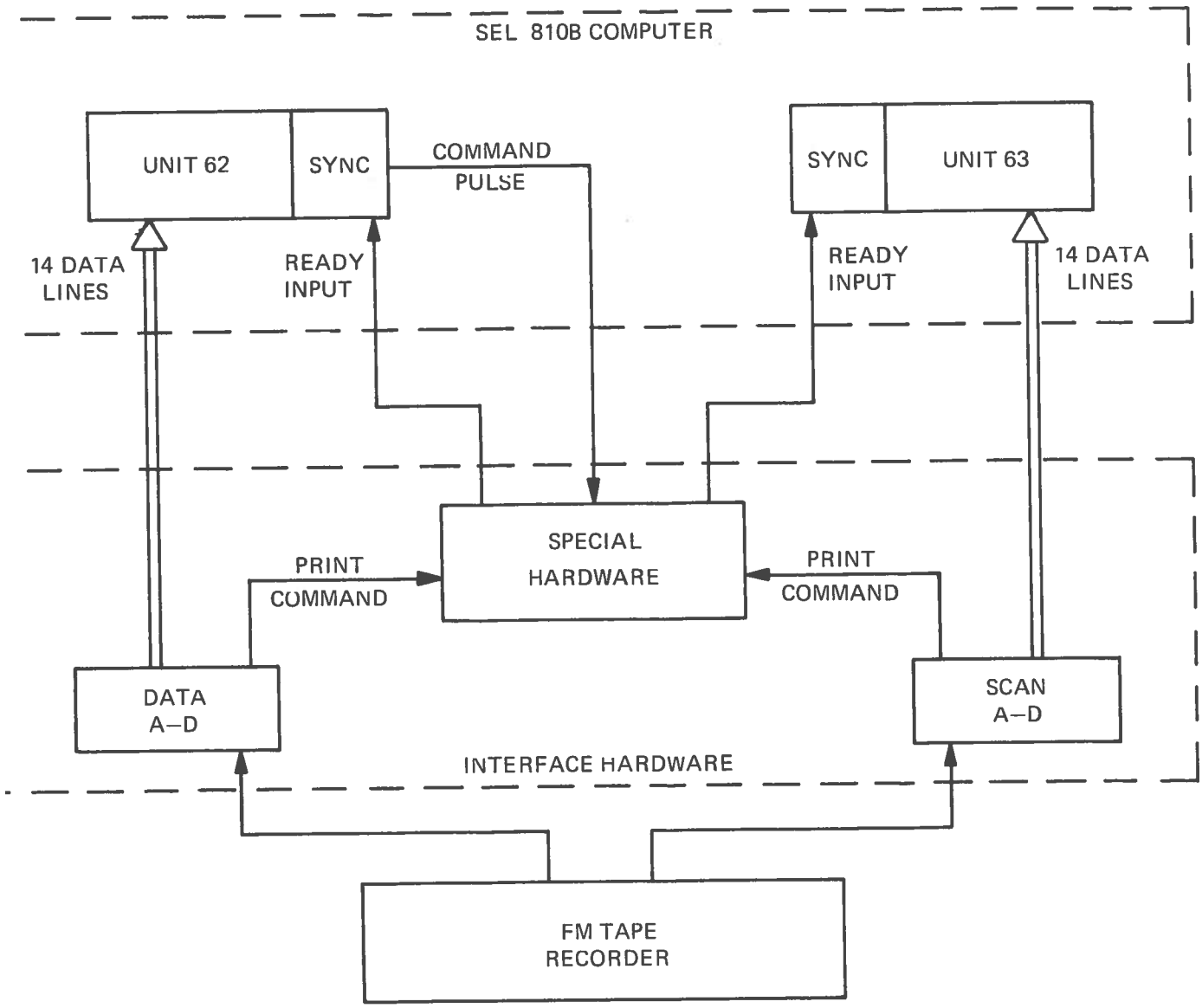

Figure 14. Block Diagram of the Computer Interface System.

logic compatible with both the A-D converters and the computer. Interface cabling diagrams are shown in Figures 16 and 17.

Section 6.2 is the computer program of the conversion routine for the polar nephelometer. This section contains flow charts, assembly listings, and sample programs.

A minor modification in the computer to polar nephelometer interface was made to have equipment automatically "shut down" at the completion of the FM recorder analog data to computer punched paper tape conversion. To actuate the automatic shutoff, a negative one volt signal previously must be recorded on the data channel at the program termination point. This can be accomplished by switching the tape recorder from the data input mode to the negative one volt calibration mode. During the recorder playback the negative one volt is sensed by the computer and the computer outputs a four volt, one microsecond pulse. This pulse actuates a unijunction monostable multivibrator which has a time period of approximately 10 seconds. The multivibrator actuates a relay which in turn removes 110 volt power from the tape recorder and thereby shuts the data conversion playback system off. Figure 18 shows a schematic of the modification.

2.9.3. ACCURACY OF THE POLAR NEPHELOMETER

The accuracy of the polar nephelometer is limited by the FM tape recorder signal/noise ratio, 40 dB, at maximum input voltage of one volt. This results in $\pm$.01 volt on both the data and scan angle channels. Neutral density filters ranging from 0 to 3.0 neutral density are automatically cycled in front of the polar nephelometer detector. This allows the detector output voltage to be in a range which will yield the best possible accuracy from the FM tape recorder.

Also by automatically cycling these neutral density filters, the FM tape recorder can be overloaded. To avoid overloading the tape recorder, a 1.4 volt limiter was placed between the data channel output and the tape recorder input. In the polar nephelometer computer-reduction routine, all signals over 1.0 volt are excluded to avoid possible ambiguity caused by the limiter. Figure 19 shows the calibration curve of the limiter.

2.9.4 CALIBRATION OF THE SPECTRAMETRICS PN-3 POLAR NEPHELOMETER

The calibration procedure of the nephelometer is based on the method given by Pritchard and Elliot (1960). The scattered light from the experimental sample is compared to

A–D CONVERTER

DIGITAL DESCRIPTION		PIN CONN.	COMPUTER CONNECTION DATA PIN	DATA CONN.	SCAN PIN	SCAN CONN.
UNITS	1	U	17	12	37	12
	2	17	15	12	35	12
	4	T	13	12	33	12
	8	16	11	12	31	12
10's	1	12	9	12	29	12
	2	11	7	12	27	12
	4	N	5	12	25	12
	8	M	3	12	23	12
100's	1	7	17	13	37	13
	2	6	15	13	35	13
	4	H	13	13	33	13
	8	F	11	13	31	13
1000		4	9	13	29	13
OVERANGE		2				
DIGITAL GND		A	GND	12 & 13	GND	12 & 13
POLARITY		B	3	(13)	23	13
CONVERSION COM.		D				
PRINT COMM.		R				
+5 V.Hs		E				
DEC. POINT	xxxxx.	V				
	xxx.s	P				
	xx.xx	J				
	x.xxx	C				

SCAN METER IS UNIT 63 OF SEL 810B.
DATA METER IS UNIT 62 OF SEL 810B.

Figure 17. List of Interface Cabling Instructions - 2.

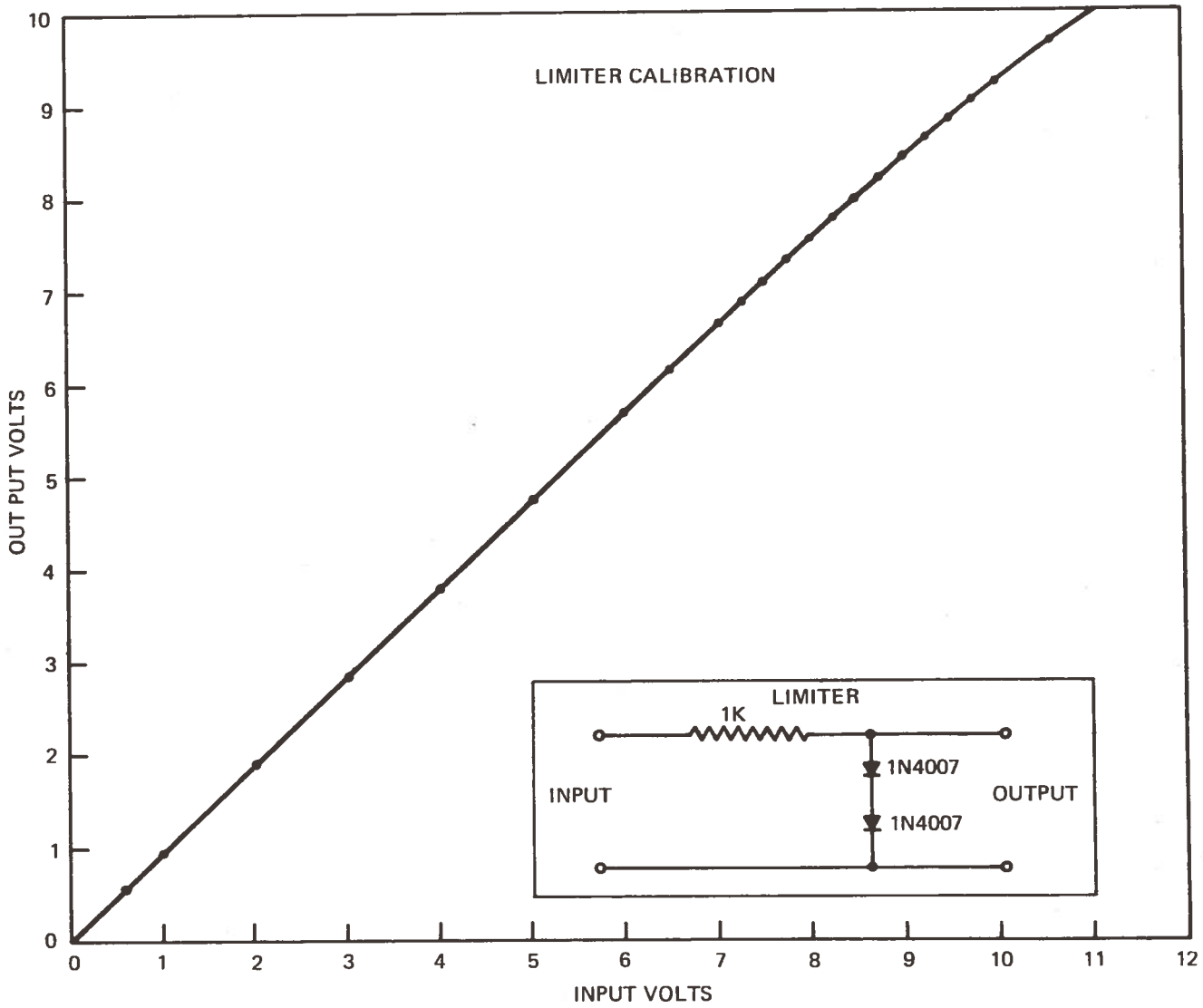

Figure 19. Calibration Curve of the 1.4 Volt Limiter between the Data Channel Output and the Tape Recorder.

a portion of light falling on the surface element dA, $\tilde{R}$ is the screen's reflectivity relative to a perfect diffuse reflector, and the integral is taken over the illuminated portion of the screen. Letting z be the coordinate normal to the area A and again neglecting the variation of γ' and γ'' over the scattering volume, we obtain from the measured function $\tilde{W}_c(z)$ the integral

$$\int W_c dz = \pi^{-1} a_{11} p_{11} C_2 R(\gamma',\gamma'') \cos\gamma' \cos\gamma'' \iiint E C_1 dv \qquad (4)$$

From Equations (2) and (4) the expression obtained for the experimental volume scattering coefficient is

$$\beta'(P,A,\theta) = \frac{\tilde{a}_{11}\tilde{p}_{11}\tilde{R}(\gamma',\gamma'') \cos\gamma' \cos\gamma''}{a_{11}p_{11}\pi \int \tilde{W}_c dz} W_s \qquad (5)$$

$$= K(P,A,\theta)\, W_s$$

We note that if the combination $\tilde{P}$ and $\tilde{A}$ is the same as P and A, the calibration coefficient reduces to

$$K(P,A,\theta) = \frac{R(\gamma',\gamma'') \cos\gamma' \cos\gamma''}{\pi \int W_c dz} \qquad (6)$$

The coefficient for any polarizer combination $\tilde{P}$ and $\tilde{A}$ at the scattering angle θ is simply related to that for the combination P and A by

$$\tilde{K}(\theta) = \frac{a_{11}p_{11}}{\tilde{a}_{11}\tilde{p}_{11}} K(\theta). \qquad (7)$$

To evaluate $K(P,A,\theta)$ by Equation (6), we must fix the absolute value of the reflectivity $R(\gamma',\gamma'')$. First, it is noted the relative reflectivity can be determined from the peak value of the response to the reflecting screen at the specific incidence and reflection angles. Assume that the source and detector beams are of identical rectangular cross section and are properly aligned (see Figure 20). Then, if $\gamma' < \gamma''$, the maximum common area on the reflecting screen falls completely within the detector beam, and the response $W_{c\ max}$ can be expressed as:

$$W_{c\ max} = \pi^{-1} a_{11} p_{11} C_2 R(\gamma',\gamma'') \cos\gamma'' C_1 I_0 , \qquad (8)$$

where

$$I_o = \iint_{A_{max}} E \cos\gamma' \, dA$$

is the total illumination in the source beam. The response $W_{c\ max}$ can be compared to the similar value for an MgO standard reflector obtained at chosen angles γ'^* and γ''^*:

$$\frac{W_{c\ max}\ (P,A,\theta)}{W^*_{c\ max}\ (P,A,\theta^*)} = \frac{R(\gamma',\gamma'')\ \cos\gamma''}{R^*(\gamma'^*,\gamma''^*)\ \cos\gamma''^*} \ . \qquad (9)$$

The accepted value of R* for MgO near normal incidence and reflection is 0.98. The calibration coefficient as a function of polarizers and scattering angle is specified completely by:

$$K(P,A,\theta) = \frac{a^*_{11}p^*_{11}\ R^*\ \cos\gamma'\cos\gamma''^*}{a_{11}p_{11}W^*_{c\ max}(\theta^*)\ W'_\theta(z)\ dz} \qquad (10)$$

where

$$W'_\theta\ (z) = W_c(z)/W_{c\ max}, \text{ with } \theta = \gamma' + \gamma''.$$

2.10 SUMMARY

The detailed description of the instrumentation used in the Laser Communication and Detection experiment was included in this report to assist anyone who might possibly want to utilize the equipment for future studies of channel impulse transmission response under fog and haze conditions.

and the magnetic field $\vec{H}$ vary harmonically in time as $e^{-i\omega t}$. The wave number k is equal to ω/c, where c is the velocity of light in vacuum. By taking the curls of the first two of Equations (1) and combining the resulting equations with the last two of Equations (1), we obtain the following field equations for $\vec{E}$ and $\vec{H}$:

$$\nabla^2\vec{E} + k^2n^2\vec{E} + 2\vec{\nabla}(\vec{E}\cdot\vec{\nabla}\ln n) = 0 \tag{2}$$

$$\nabla^2\vec{H} + k^2n^2\vec{H} = 0 \tag{3}$$

where $\varepsilon = n^2$ and n is the index of refraction.

Equations (2) and (3) govern the propagation of any harmonic electromagnetic wave through an arbitrary inhomogeneous medium. In our case, we are interested in optical wave propagation through a weakly turbulent atmosphere whose index of refraction can be represented as follows:

$$n(\vec{r}) = 1 + n_1(\vec{r}) \tag{4}$$

where n_1 is a small random perturbation ($|n_1| \ll 1$). At optical frequencies, the fluctuations, n_1, in the index of refraction are due primarily to random atmospheric temperature fluctuations.

Some of the statistical characteristics of the random field $n_1(\vec{r})$ should be mentioned. First of all, the mean value of n_1 denoted by $\bar{n}_1$ is identically zero. The average designated by the horizontal bar is to be interpreted as an ensemble average over all realizations of the random field n_1. Secondly, $n_1(\vec{r})$ is generally assumed to be locally isotropic. That is to say, the various statistical moments of the random function $g(\vec{r}_1,\vec{r}_2) = n_1(\vec{r}_1) - n_1(\vec{r}_2)$ depend only upon $r = |\vec{r}_1 - \vec{r}_2|$ provided that r is sufficiently small. The upper limit on the separation distance r for which atmospheric turbulence is isotropic is generally designated in the literature by L_o and is often referred to as the outer scale of the turbulence. This parameter is best interpreted as the linear dimension of the largest inhomogeniety for which the assumption of isotropy is valid. The length L_o is typically on the order of several meters near the earth's surface and tends to increase slowly with altitude. Another important scale length relating to atmospheric turbulence is the inner scale of the turbulence. This parameter, which is generally designated by ℓ_o, is the linear dimension of the smallest inhomogeniety or turbulent eddy. The length ℓ_o is typically on the order of a few millimeters near the earth's surface and, like L_o, increases slowly with altitude.

It is a simple matter to show that Equation (7) can be rewritten in terms of $\psi \equiv \ln u$ as follows:

$$\nabla^2\psi + (\nabla\psi)^2 + k^2 (1 + n_1)^2 = 0, \tag{8}$$

where use has been made of Equation (4). Let A and S denote, respectively, the amplitude and phase of the wave field u. That is to say, $u = Ae^{iS}$. Clearly, the following relationships hold among ψ, A, and S:

$$\begin{aligned} \mathrm{Re}(\psi) &= \ln A \\ \mathrm{Im}\ \psi &= S \end{aligned} \tag{9}$$

We will assume that in the absence of any turbulence ($n_1 \equiv 0$), ψ would reduce to a function ψ_o which satisfies the unperturbed wave equation.

$$\nabla^2\psi_o + (\nabla\psi_o)^2 + k^2 = 0 \tag{10}$$

As a result of the turbulence, ψ_o is subject to a random perturbation ψ_1 ($|\psi_1| << |\psi_o|$). Substituting $\psi = \psi_o + \psi_1$ into the wave equation (8) and using Equation (10), we obtain the following equation for the perturbation ψ_1:

$$\nabla^2\psi_1 + \vec{\nabla}\psi_1 \cdot (2\vec{\nabla}\psi_o + \vec{\nabla}\psi_1) + 2k^2 n_1 + k^2 n_1^2 = 0 \tag{11}$$

We now make use of the fact that in clear weather, $|n_1| << 1$ to linearize Equation (11) by dropping the terms $(k^2 n_1^2)$ and $(\nabla\psi_1 \cdot \nabla\psi_1)$. The resulting linear equation is

$$\nabla^2\psi_1 + 2\nabla\psi_o \cdot \nabla\psi_1 + 2k^2 n_1 = 0 \tag{12}$$

The random perturbation ψ_1 governed by Equation (12) has a very simple interpretation. Let $u_o = e^{\psi_o}$ denote the wave field in the absence of turbulence, and let A_o and S_o denote, respectively, the amplitude and phase of u_o. The following relationships hold among u_o, A_o and S_o (cf. Equation (9)):

$$\begin{aligned} \mathrm{Re}(\psi_o) &= \ln A_o \\ \mathrm{Im}(\psi_o) &= S_o \end{aligned} \tag{13}$$

Applying Equations (13) and (9) and recalling that $\psi_1 = \psi - \psi_o$, we find that

$$\begin{aligned} \mathrm{Re}(\psi_1) &= \ln(A/A_o)\ , \\ \mathrm{Im}(\psi_1) &= S - S_o \end{aligned} \tag{14}$$

follows:

$$\psi_1(\vec{r}) = \sum_i \int_{V_i} n_1(\vec{r}') \, G(\vec{r},\vec{r}') d\vec{r}' \quad . \tag{17}$$

Since the cells V_i have linear dimensions on the order of L_o, the fluctions n_1 between cells and hence the integrals appearing in Equation (17) are uncorrelated. Therefore, ψ_1, as given by Equation (17), is the sum of a large number of uncorrelated random variables all having the same probability distribution. By the central limit theorem, the probability distribution of such a sum approaches a Gaussian, as the number of terms in the series increases without bound. Since L_o is typically on the order of a few meters near the earth's surface, one can anticipate there being a very large number of cells V_i for most optical propagation paths of interest. Consequently, we arrive at the important result that both $\ln(A/A_o) = \mathrm{Re}(\psi_1)$ and $(S-S_o) = \mathrm{Im}(\psi_1)$ should approximate Gaussian random variables rather closely. Furthermore, if $\ln (A/A_o)$ had a Gaussian distribution, then A/A_o would have a log normal distribution, as would $I/I_o = (A/A_o)^2$ where I denotes the actual wave intensity and I_o denotes the intensity which would be observed in the absence of turbulence. In fact, log normal distributions for intensity fluctuations have been reported by several experimenters, thus confirming a major feature of the Tatarski theory (Tatarski, 1961; Fried, Mevers, and Keister, 1967).

With the preceding general comments regarding the statistics of ψ_1 as a preface, we will now proceed to consider some specific examples of optical wave propagation in a turbulent medium. In particular, the cases of plane and spherical wave propagation will be discussed in some detail.

3.3.2 PLANE WAVES

To study plane wave propagation in a turbulent atmosphere, we substitute $u_o = A_o e^{ikx}$ into Equation (15). The turbulent medium is envisioned as occupying the half space $x>0$ with the observation point lying in the plane $x=L$. Reflections can be ignored in clear weather so that the volume of integration in Equation (15) lies between the planes $x=0$ and $x=L$. In fact, Tatarski noted that the largest angle of scattering of energy by the refractive index inhomogenieties is on the order of λ/ℓ_o, which, as noted earlier, is very much less than one in clear air at optical frequencies. As a consequence, the volume of integration can be further restricted to a cone with a vertex at the observation point and with an aperture angle given by λ/ℓ_o. This small angle approximation con-

turbulence:

$$D_s(\rho) = 2.91\ k^2\ LC_n^2\ \rho^{5/3}\ ((\lambda L)^{1/2} \leq \rho \leq L_o)$$
$$D_s(\rho) = 1.72\ k^2\ C_n^2\ \ell_o^{-1/3}\ L\rho^2\ (\rho << \ell_o) \qquad (25)$$

The phase structure function will play an important role in the discussion of laser pulse broadening in clear air.

3.3.3 SPHERICAL WAVES

To study the scattering of spherical waves by a turbulent atmosphere, we substitute $u_o = \frac{B}{r}e^{ikr}$ into Equation (15). As in the case of plane waves, the turbulence is envisioned as occupying the half space $x>0$. The source of the spherical wave is located at the origin and the observation point is in the plane $x=L$. The small angle approximation discussed earlier can be applied to facilitate the evaluation of the appropriate integrals.

For $(\lambda L)^{1/2} >> \ell_o$, Tatarski obtains the following expression for the log amplitude variance σ_ℓ^2 for spherical wave propagation in Kolmogorov-Obukhov turbulence:*

$$\sigma_\ell^2 = .13\ C_n^2 k^{7/6} L^{11/6} \qquad (26)$$

Comparing Equations (26) and (20), we see that the functional dependence of σ_ℓ^2 upon wave number and range is the same for both spherical and plane waves. The two expressions differ only by a numerical factor, σ_ℓ^2 being about 2.4 times as large for plane waves as for spherical waves for a given wave number and range. As was the case for plane waves, conservation of energy requires that the average measured intensity equal the intensity which would be measured in the absence of turbulence ($\overline{I}=I_o$). As was the case for plane waves, this requirement leads to the condition that $\overline{\chi} = -\sigma_\ell^2$. Equation (23) which relates the intensity and log amplitude variances for plane waves applies also for spherical waves (Equation (23)).

It should be noted that the theoretical results presented so far for plane and spherical waves can in many cases

---

*Note that this expression for σ_ℓ^2 applies for those points in the plane $x=L$ which are located at distances from the x-axis which are small compared with L.

3.4 APERTURE EFFECTS

Having outlined the main features of the Tatarski theory of light scattering by a turbulent atmosphere, we now turn our attention to various phenomena associated with the size of the receiving aperture. The investigation of these aperture-related effects is the principal objective of our experimental program.

To begin, suppose there is a circular collecting aperture of area A and diameter D lying in the plane x=L. The total signal, S, collected by this aperture is given by

$$S = \int_A I \, dA \tag{27}$$

where I is the light intensity and the integral is taken over the surface of the aperture. From the Tatarski theory, we know that I is log normally distributed at every point on the receiving aperture. If the intensity fluctuations were perfectly correlated over the entire aperture, then clearly the signal S would also be log normally distributed. However, the intensity fluctuations at two arbitrary points $\vec{r}_1$ and $\vec{r}_2$ in the plane x=L are not perfectly correlated. In fact, we can define an intensity coherence length, d, which varies inversely with the strength of the turbulence and has the property that for $|\vec{r}_1-\vec{r}_2|<d$, $I(\vec{r}_1)$ and $I(\vec{r}_2)$ are highly correlated while for $|\vec{r}_1-\vec{r}_2|>d$, $I(\vec{r}_1)$ and $I(\vec{r}_2)$ are essentially uncorrelated. This coherence length is typically on the order of $(\lambda L)^{1/2}$ for plane and spherical waves.

Clearly, if the diameter, D, of the collecting aperture is less than d, then the intensity fluctuations will be correlated over the entire surface of the aperture and S will be log normally distributed. However, if D is much greater than d, the surface of the aperture will contain a large number $N=D^2/d^2$ of coherence cells, each of diameter d, with the property that the intensity fluctuations between cells are uncorrelated. In that case, the total received signal S as given by Equation (27) would be obtained by summing up a large number of contributions from the various coherence cells, contributions which are uncorrelated with one another; therefore, by the central limit theorem, S would be a Gaussian random variable. We can therefore expect to see a variation in the signal probability density from log normal to Gaussian as the diameter of the collecting aperture increases. The predicted variation of signal statistics with aperture size is one of the phenomena we wish to investigate experimentally.

Substituting the expression for σ_X^2 given in Equation (34) into Equation (33) and making use of Equation (23), we finally obtain the following expression for $\sigma_S^2/\bar{S}^2$:

$$\sigma_S^2/\bar{S}^2 = \theta \exp(4\sigma_\ell^2) - 1 \tag{35}$$

where

$$\theta = d^2/D^2 \tag{36}$$

The quantity θ is referenced in the literature as the aperture averaging factor. According to Equation (36), this factor is inversely proportional to the square of the aperture diameter. Some caution must be applied in using Equation (36) since the assumptions leading up to it are somewhat unrealistic. In particular, the intensity fluctuations will never be *perfectly* correlated over each coherence cell and totally uncorrelated between cells. Nevertheless, Fried's (1967A) exact calculation of the aperture averaging factor for plane waves indicates that θ does vary essentially as D^{-2} for values of D greater than the coherence length. The main point to be made is that for a given set of turbulent conditions, the percentage signal fluctuation can be reduced by increasing the size of the aperture, the normalized signal variance ($\sigma_S^2/\bar{S}^2$) varying approximately as D^{-2}.

The final aperture-related phenomenon we will investigate is laser pulse broadening in clear air. Pulse broadening (channel time spread) for small receiving apertures ($D < (\lambda L)^{1/2}$) comes about primarily as a result of multipathing due to ray scattering from the index of refraction inhomogenieties. As the aperture size increases, this multipathing becomes much larger. For the larger apertures ($D > (\lambda L)^{1/2}$), however, the multipathing is not due primarily to ray scattering but rather to unscattered rays which traverse different atmospheric paths to reach different points on the receiving aperture. Since these unscattered rays traverse different atmospheric paths, they encounter different refractive index inhomogenieties (different values of n_1), and consequently the propagation times from transmitter to the receiver for these rays will differ. To get an estimate of the amount of broadening to be expected, we will adopt Brookner's (1970) formulation of the problem and introduce the structure function $D_\tau(\rho)$ for the propagation time. This structure function for two points $\vec{r}_1$ and $\vec{r}_2$ on the aperture is defined as follows:

$$D_\tau(\rho) = \overline{[\tau(\vec{r}_1) - \tau(\vec{r}_2)]^2} \tag{37}$$

3.5.1 PULSE-BROADENING MEASUREMENTS

A series of laser pulse-broadening measurements was made using the full 30 cm aperture of the Cassegrain telescope. No pulse broadening was detectable greater than the 20 picosecond resolution of our equipment. This result is consistent with the predictions of the Tatarski theory. In Section 3.4, an expression for the rms time spread, T, associated with a collecting aperture of diameter ρ was developed for plane waves propagating in Kolmogorov-Obukhov turbulence. It was shown that $T=[D_\tau(\rho)]^{1/2}$ where $D_\tau(\rho)$ is given by

$$D_\tau(\rho) = 2.91 \frac{L}{c^2} C_N^2 \rho^{5/3} (\rho \geq (\lambda L)^{1/2}) \qquad (40)$$

In our case, the path length L is 768 m and the diameter ρ is 30 cm. Substituting these values into Equation (40) and assuming that the turbulence is very strong ($C_N^2 = 5 \times 10^{-13}$ $m^{-2/3}$), we obtain the following estimate for the time spread T:

T = .04 picosecond

This estimated broadening is almost three orders of magnitude below the resolution of our equipment.

3.5.2 SIGNAL PROBABILITY DISTRIBUTIONS AND APERTURE AVERAGING

To determine ths signal probability distribution for a given aperture, a large number of pulses were first analyzed to determine the average horizontal position of the pulse height maximum. The pulse heights at this position were then recorded for a period of approximately one minute. The sample size after one minute of observation was approximately 2.5×10^4. A computer then calculated the signal probability density by dividing the number of pulse heights observed at each of the 255 vertical scope levels by the sample size. A separate computer program calculated the cumulative signal distribution. Using the calculated signal probability density, the computer then calculated the signal mean ($\bar{M}$), variance (σ_M^2) and normalized variance ($\sigma_M^2/\bar{M}^2$). The letter "M" is used here to denote the measured signal which is the sum of the laser signal, background noise, and the d.c. bias introduced by the electronics. The laser was then blocked off at the transmitter, and the background noise probability distribution at the same horizontal scope position was determined. The sampling time for the determination of the noise distribution was about one minute. The cumulative noise distribution also was determined along with the noise mean ($\bar{N}$), variance (σ_N^2) and the normalized variance ($\sigma_N^2/\bar{N}^2$). The quantity $\bar{N}$ is of course the average background noise plus the d.c. bias intro-

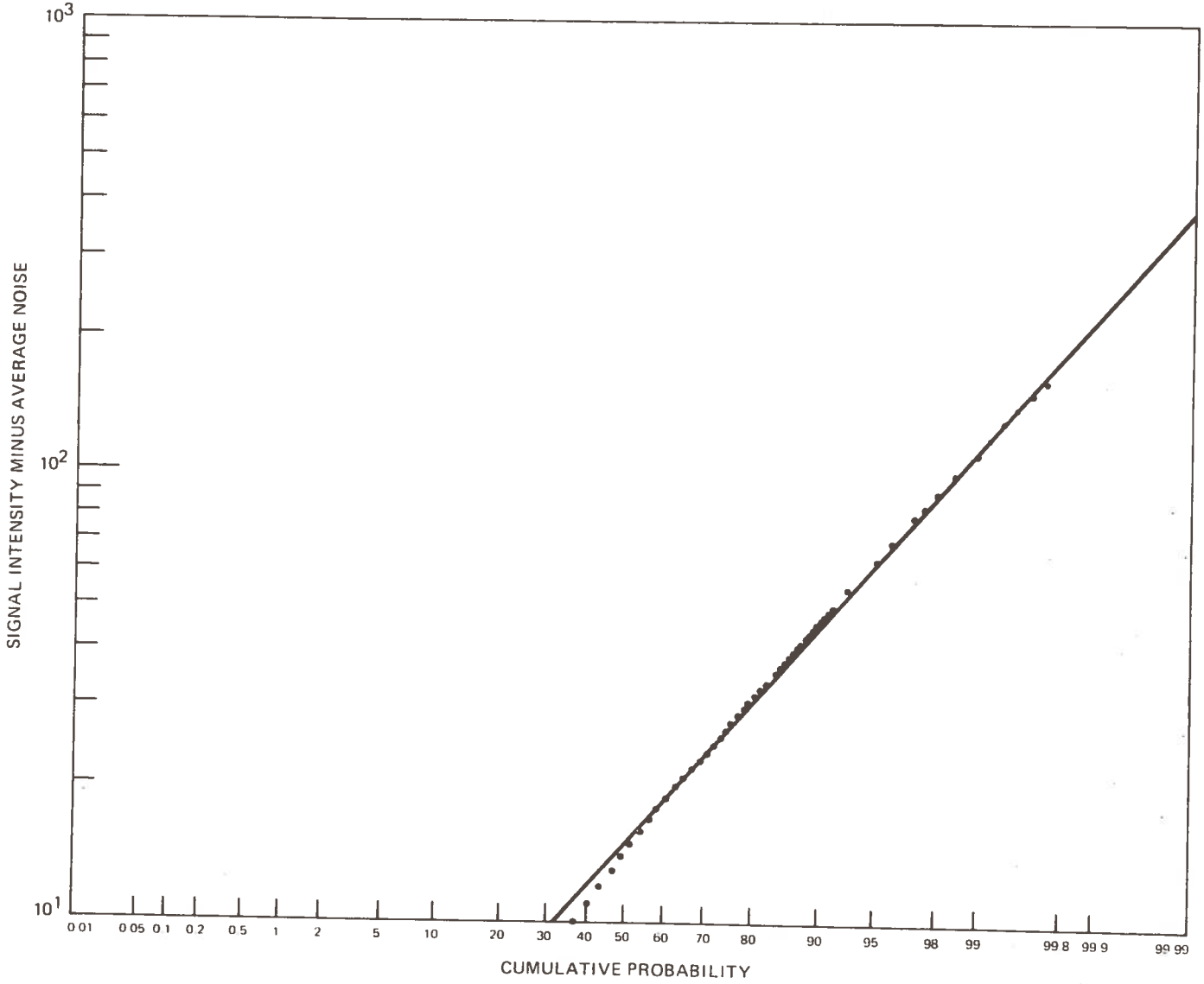

Figure 21. Cumulative Probability Distribution of the Measured Signal Versus the Measured Signal Minus the Average Noise for a 1-Cm Aperture.

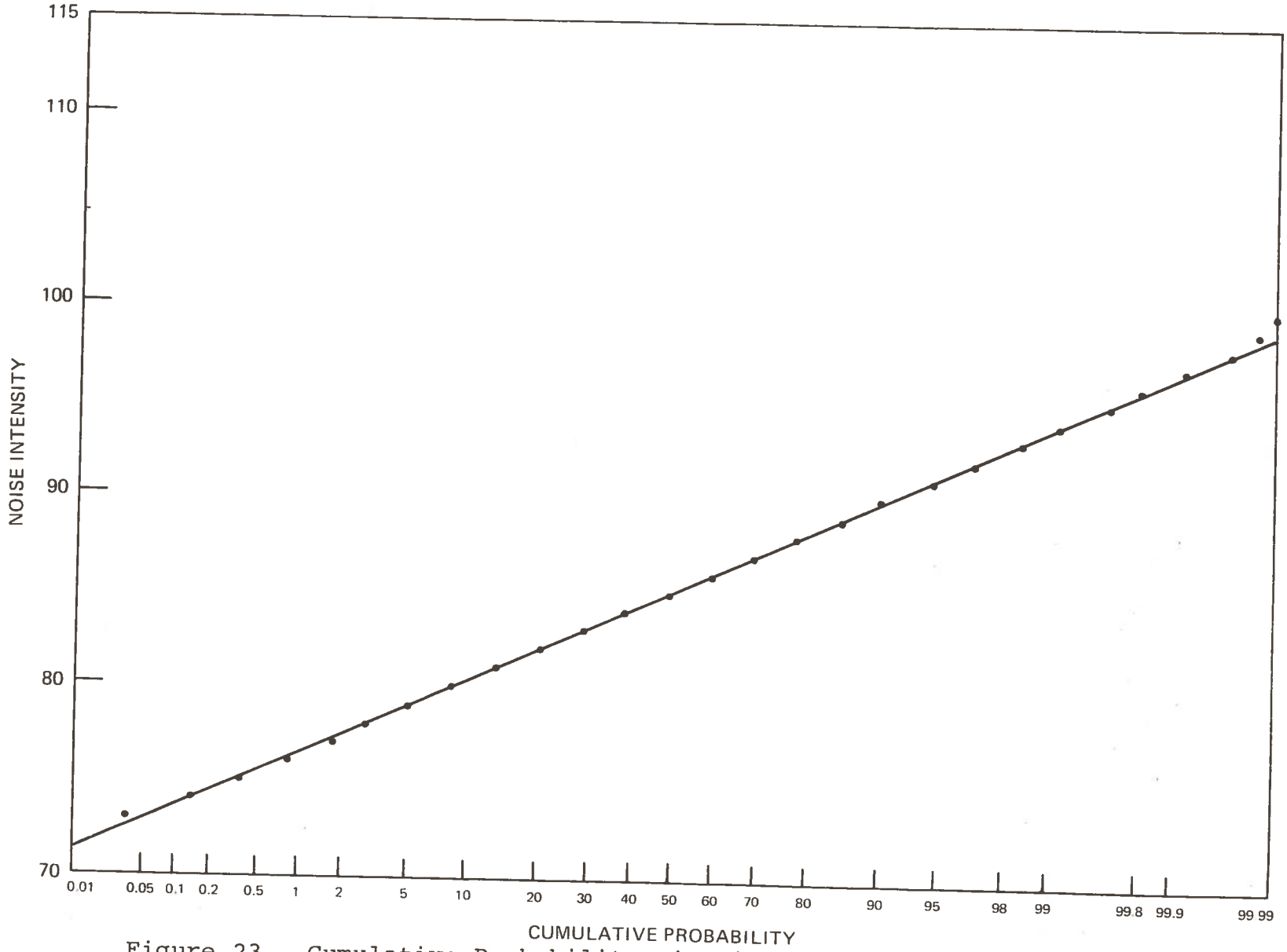

Figure 23. Cumulative Probability Distribution of the Noise Level Measured with a 30-Cm Aperture.

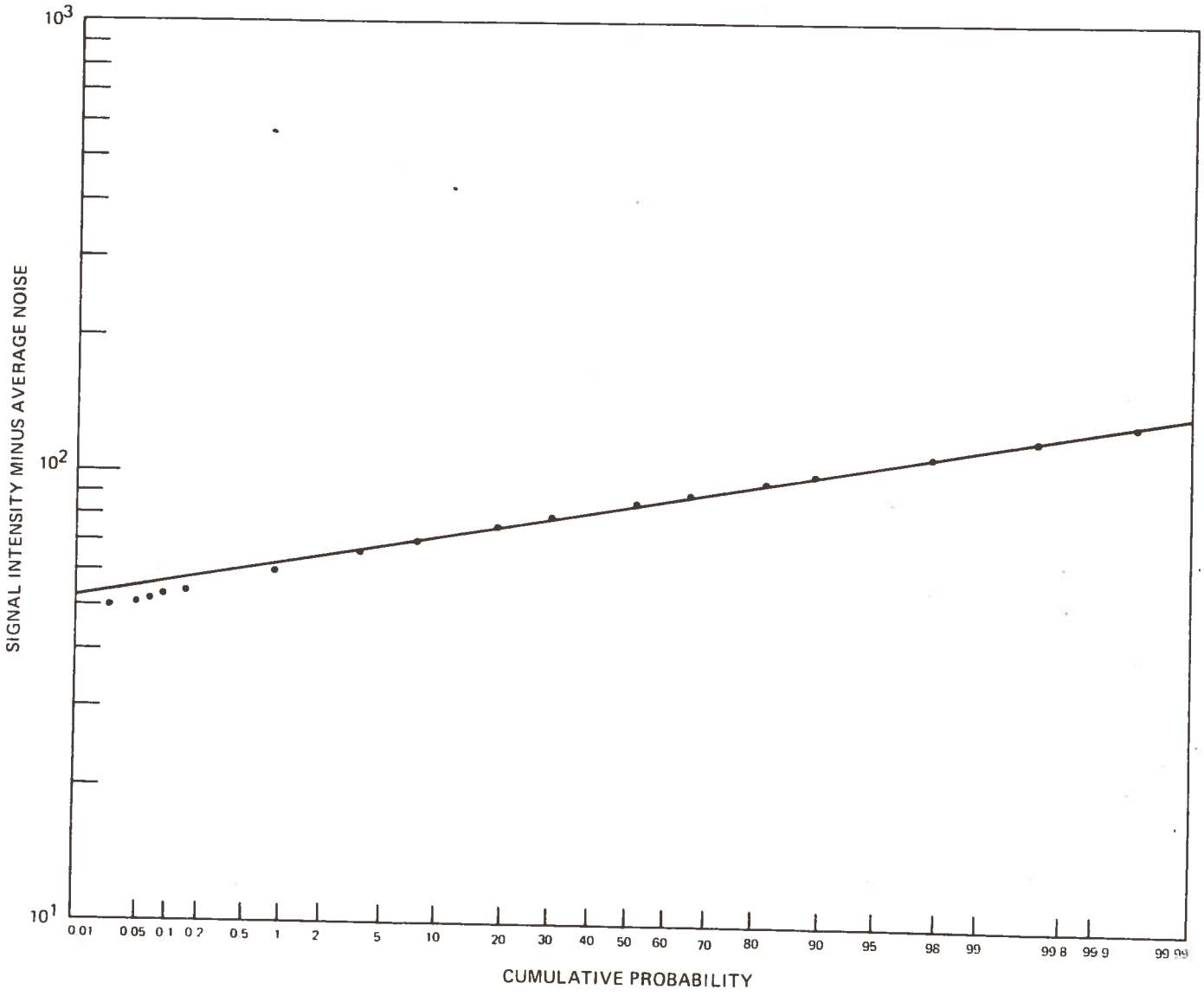

Figure 24. Cumulative Probability Distribution of the Measured Signal Versus the Measured Signal Minus the Average Noise for a 30-Cm Aperture.

tribution should be Gaussian.

The obvious inference to be drawn from the persistence of the log normal signal distribution for large apertures is that the intensity coherence length is much longer than the Tatarski theory for either plane or spherical waves predicts. This conclusion is further supported by the curves shown in Figures 26 add 27 where we have plotted the normalized scintillation variance ($\sigma_S^2/\bar{S}^2$) as a function of aperture diameter.* The data depicted in these graphs were recorded on separate days. The point scatter observable in both graphs is probably due to the fact that turbulence conditions varied during the course of each run. A complete set of measurements required nearly 90 minutes. These curves illustrate the phenomenon of aperture averaging. The normalized variance is seen to decrease as the diameter of the collecting aperture increases. According to the theory developed in Section 3.4, the normalized variance should vary as D^{-2} for values of D greater than the coherence length. In fact, the two curves plotted in Figures 26 and 27 do vary roughly as D^{-2} for values of D in excess of 10 cm. From this observation, we might conclude that the coherence length is indeed larger than 10 cm, then the 30 cm collecting aperture would probably contain too few coherence cells for there to be any noticeable deviation from log normality of the signal distribution.

3.6 SUMMARY

We performed a series of measurements of light scattering by clear air turbulence. The purpose of this measurement program was twofold: first of all, we wanted to measure pulse broadening due to multipathing in clear air, and secondly, we wanted to study the dependence of scintillation statistics upon the size of the collecting aperture.

The pulse-broadening measurements were carried out using the largest collecting aperture available to us (30 cm), since, according to the theory, broadening increases almost linearly with aperture diameter. No pulse broadening was detectable greater than the 20 picosecond resolution of our equipment.

---

*For the larger collecting apertures, the effective collecting area is somewhat reduced owing to the presence of the secondary mirror of the Cassegrain telescope which blocks off part of the beam. The secondary mirror is 10 cm in diameter. Consequently, the effective diameter of the full aperture is about 28.3 cm rather than 30 cm. The smaller apertures were placed off axis to avoid this problem.

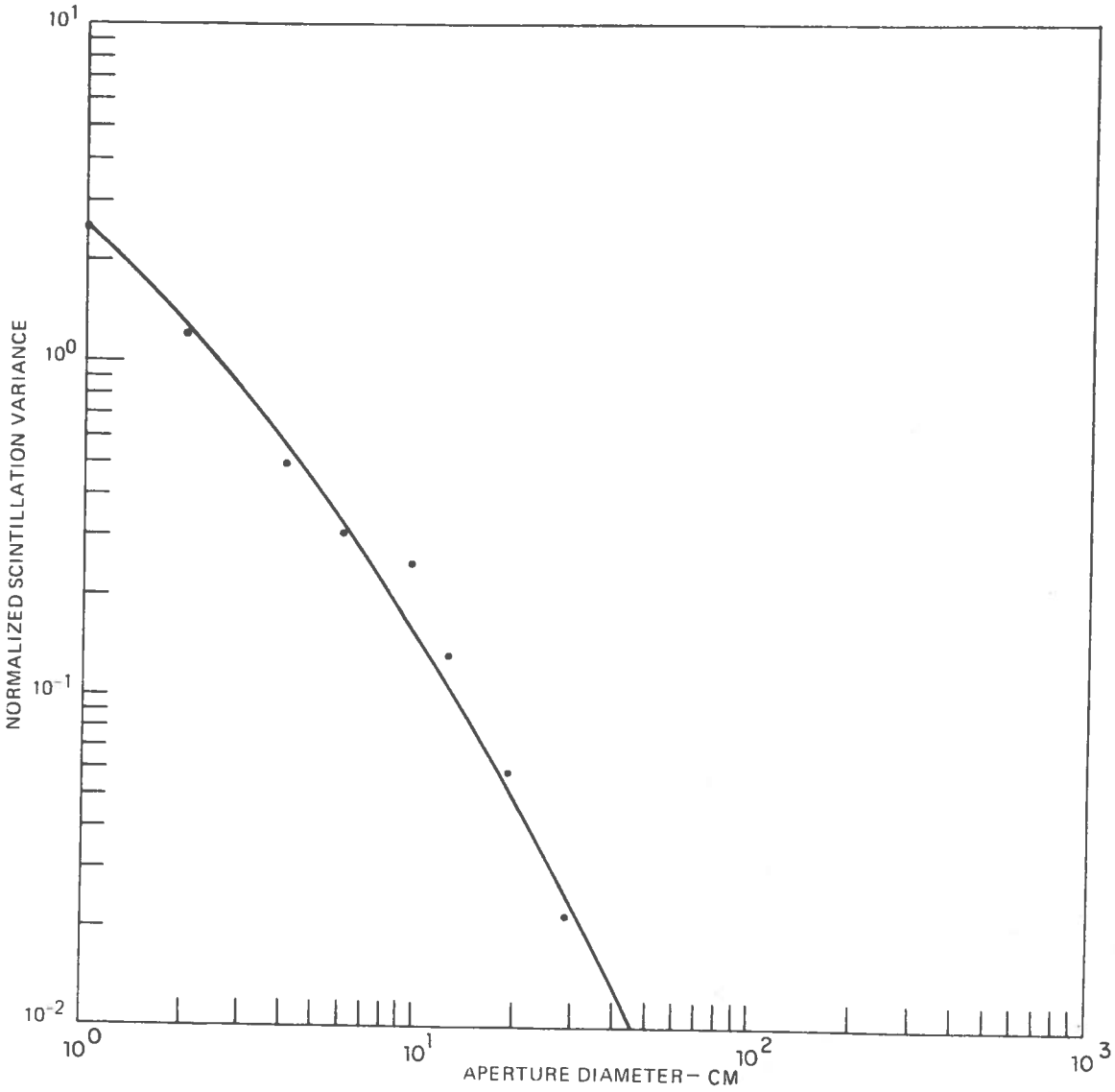

Figure 27. Normalized Scintillation Variance Versus Aperture Diameter.

4. CHARACTERIZATION OF OPTICAL COMMUNICATION CHANNELS IN SCATTERING MEDIA

4.1 INTRODUCTION

The clear natural atmosphere is potentially an omnibus communication channel for a great portion of the optical spectrum offering very salient characteristics, notably: bandwidths of perhaps 10^{12} Hz(1THz) and compactness of transmission/reception hardware. However, any unprotected atmospheric optical communication link must contend with varying degrees of signal fading and dispersion caused by random signal scattering effects occasioned by transitory hazes, fogs, pollution, etc. It has been experimentally demonstrated that channel bandwidth and gain can be seriously degraded under typical poor visibility conditions, and also that such problems can be partially dealt with by system over-design. (Chu and Hogg, 1968; Bucher, Lerner, and Niessen, 1970; Gilder and Hao, 1970; Kerr, Titterton and Brown, 1969). However, the available data are in general not complete enough for even tentative prediction of a communication link's performance under specified atmospheric conditions.

The objective of this part of the present work is to report atmospheric channel signal transmission characteristics and simultaneously measured volume scattering parameters which together are adequate to characterize the performance of a class of communication links under a range of specified conditions. Though the experimental data are restricted by limitations of the test site, available hardware, etc., the results can be applied to a general set of communication link design problems.

4.1.1 COMMUNICATION LINK GEOMETRICAL PARAMETERS

The characterization of an optical scatter communication channel requires specification of the geometry of the transmitter/receiver link as well as the disposition, density, and light-dispersing properties of the scattering medium. Typical atmospheric optical communication systems currently under development cover a wide scope, including: ground-to-space links through prevailing cloud strata, over-the-horizon or indirect transmission by light scattering from clouds, ground-to-ground line-of-sight links restricted by the intervening scattering and turbulence, etc. Applicability of the present work is limited to line-of-sight optical links where the transmitter and receiver are immersed in a homogeneous, isotropic scattering

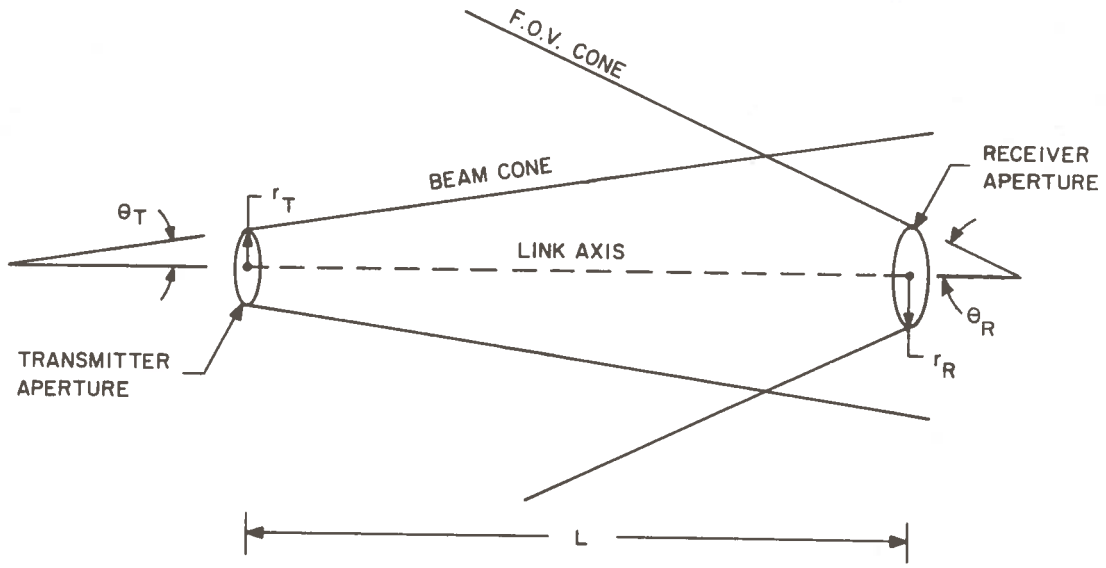

Figure 28. Simplified Geometrical Concept of a Line-of-Sight Optical Communication Link. (The Scale Invariants are: $\Omega_T = 2\pi(1-\cos\theta_T)$, $\Omega_R = 2\pi(1-\cos\theta_R)$, $C_T = \pi r_T^2/L^2$, and $C_R = \pi r_R^2/L^2$.)

coefficients. To this purpose we employ a portable recording polar nephelometer located in the open air at the experimental range.

Such a device is shown schematically in Figure 29. The instrument responds to light which is scattered by approximately the angle θ from the source beam into the detector beam. Measurements can be taken with combinations of six basic types of polarizing filters placed at the source and at the detector. The basic filters include four linear and two circular polarizers: horizontal - H, vertical - V, diagonals - D, d, right circular - R, and left circular - L. The diagonals D and d are obtained by rotating the vertical polarizer V clockwise and counterclockwise by 45° respectively, when looking in the direction of propagation. Right and left circular polarization also refer to clockwise and counterclockwise, respectively, looking in the direction of propagation. When properly calibrated, the instrument response is proportional to the volume differential scattering coefficient βs (P, A, θ) of the ambient medium for the specific polarizer-analyzer combination chosen. The Mueller matrix for an isotropic medium can be determined from measurements of β_α for six independent P-A combinations. With the selection HH, VV, HV, dd, DR, RR the non-zero elements of the matrix are given by:

$$M_{11} = \tfrac{1}{2}\beta_{HH} + \tfrac{1}{2}\beta_{VV} + \beta_{HV} \qquad (2a)$$

$$M_{22} = \tfrac{1}{2}\beta_{HH} + \tfrac{1}{2}\beta_{VV} - \beta_{HV} \qquad (2b)$$

$$M_{33} = 2\beta_{dd} - M_{11} \qquad (2c)$$

$$M_{44} = 2\beta_{RR} - M_{11} \qquad (2d)$$

$$M_{12} = M_{21} = \tfrac{1}{2}\beta_{HH} - \tfrac{1}{2}\beta_{VV} \qquad (2e)$$

$$M_{34} = -M_{43} = M_{11} - 2\beta_{DR} \qquad (2f)$$

It can be shown that the element M_{11} is the differential scattering coefficient for unpolarized light β_{uu} ($= \beta_s(\theta)$) which is the only quantity of interest for unpolarized transmission systems.

One limitation of this approach to fog characterization should be mentioned here. At the He-Ne laser wavelength of 6328Å the differential scattering coefficients of nearly all natural aerosols are sharply peaked at small forward angles. It is difficult to measure this forward scattering because of the problem of isolating the direct beam. The nephelometer used in the present experiment has an angular range of 20° to 155°, whereas it appears from numerical

estimates given by Kattawar and Plass (1968, Figure 1) that variations in scattering coefficient of perhaps two orders of magnitude occur for angles less than 5°. It is clear that our nephelometer data cannot be simply extrapolated without further knowledge. A useful additional constraint on measured scattering data is found by noting that the absorption coefficient β_α may be neglected in comparison with the total scattering coefficient

$$\beta_s = 2\pi \int_{-1}^{1} \beta_s(\theta)\, d\cos\theta \qquad (3)$$

$$\simeq \beta_e$$

for the expected experimental conditions. Thus if the extinction coefficient β_e can be measured, it becomes possible to choose smooth extrapolations of $\beta_s(\theta)$ which approximately fit the integral of Equation (3). The problems of measuring β_e under multiple scattering conditions have already been noted. Holland* has suggested that the scattering data obtained in the nephelometer angular range can be fit to a model droplet size distribution and then the forward angle scattering functions calculated as in Kattawar and Plass (1968). Implementation of this procedure is beyond the scope of the present work.

We conclude that complete specification of a homogeneous optical scatter channel must include measurement of the Mueller scattering matrix $M_{ij}(\theta)$ (or at least the unpolarized differential scattering coefficient $\beta_s(\theta)$) and the optical thickness $\beta_e L$ of the transmitter/receiver path, in addition to the geometrical parameters of the previous section.

4.1.3 CHARACTERIZATION OF CHANNEL TIME AND FREQUENCY DISPERSION

In the process of transmitting a signal over an optical communication link, an amount of energy is radiated into the channel in a certain mode or pattern from the transmitter aperture. A portion of this signal energy together with added energy from background noise sources falls on the receiver aperture. This combined energy is processed by means of lenses, filters, etc., and ultimately, the occurrence and form of the original signal is determined with a certain efficiency by a detector. The performance of such a communication link is usually characterized by some measure such as the probability of error (or in the analog case, the r.m.s. error) as a

---

*Private communication

Having in mind applications to direct detection systems, we postulate that the receiver is a hypothetical square-law envelope detector with a response to the received amplitude given by:

$$j_r(t) = \int_{-\infty}^{\infty} dt' b_F(t-t')\, r(t)^2 \qquad (7)$$

where $b_f(t)$ is the response of a perfect low-pass filter of bandwidth $F<F_o$,

$$b_F(t) = \sin 2\pi Ft/\pi t$$

Henceforth, we shall denote such convolution integrals as Equation (7) by the notation $b_F * r(t)^2$.

The adoption of this detector model implies that all functions are defined over the entire infinite time domain. For our purposes, the conclusions of the ensuing analysis remain sufficiently valid, when applied to signal transmission during a finite time interval, if the time bandwidth product is large ($TF>>1$).

With the above detector, the expected output for a given transmitted signal $s(t)$ can be expressed in the form:

$$\overline{j_r(t)} = \int_o^{\infty} d\tau\ \phi(0,\tau)\, j_s(t-\tau) + \overline{n(t)^2} \qquad (9)$$

where:

$$\phi(T,\tau) = \overline{h(t,t-\tau)\ h(t+T,\ t+T-\tau)} \qquad (10)$$

$$j_s(t) = b_F * S(t)^2 \qquad (11)$$

We may imagine $s(t)$ to be a narrowband signal of the form

$$s(t) = V(t) \cos(\Omega t + \delta) \qquad (12)$$

where the bandwidth f_o of the envelope $V(t)$ and the bandwidth of the detector satisfy the relation

$$2f_o < F < \Omega/\pi. \qquad (13)$$

The function $j_s(t)$ is then just the squared signal envelope $V(t)^2$.

scattering function, the received amplitude power spectrum reduces to:

$$P_r(f) = N(f) + \Sigma |V_n^2| \int d\tau \, (\sigma(f-\Omega/2\pi - nf_o, t) + \sigma(f + \Omega/2\pi - nf_o, \tau)) \tag{17}$$

where $N(f)$ is the spectral density of the background noise and V_n is the Fourier expansion coefficient of the signal envelope

$$V(t) = \Sigma V_n \, e^{2\pi i n f_o t} \tag{18}$$

The channel scattering function for Doppler shift f_D and time delay τ is the Fourier transform of the impulse spread covariance

$$\sigma(\tau, f_D) = \int e^{-i\omega_D t} \, \phi(t,\tau) dt \quad ; \; \omega_D = 2\pi f_D. \tag{19}$$

To measure the amplitude power spectrum of Equation (17) it would be necessary to analyze the received beam with a high resolution optical spectograph.

By contrast, the power spectrum of the detected intensity $b_F * T(t)^2$ may be shown to take the form

$$P_{b*r^2}(f) = 2 \, (\overline{r^2})^2 \, \delta(f)$$

$$+ 4N\{n^2 + 2\Sigma |V_n|^2 \int \phi \, (O,\tau) d\tau\}$$

$$+ 4 \sum_m \sum_n |V_n \, V_{m-n}|^2 \, x$$

$$\int d\tau \int d\tau' \int df' \quad \sigma(f',\tau) \quad \sigma(f-mf_o-f', \tau') \tag{20}$$

This spectrum has the appearance of a series of peaks unequal in height but uniform in width. The width will be assumed to be roughly twice the Doppler bandwidth of the scattering function. The estimate of time dispersion in Equation (14) is relatively meaningful only when broadening of pulses over the optical link is significant compared to the initial pulse width. The effects of refractive dispersion, clear air turbulence, and single-scatter multipathing have been shown to be clearly insignificant compared to our available 1 nanosecond pulses (Kerr, Titterton, and Brown, 1969). The influence of multiple scattering is possibly significant, but this is difficult to estimate. The results which have been obtained by various numerical techniques seem to depend heavily on the link geometrical parameters assumed (Kerr, Titterton, and

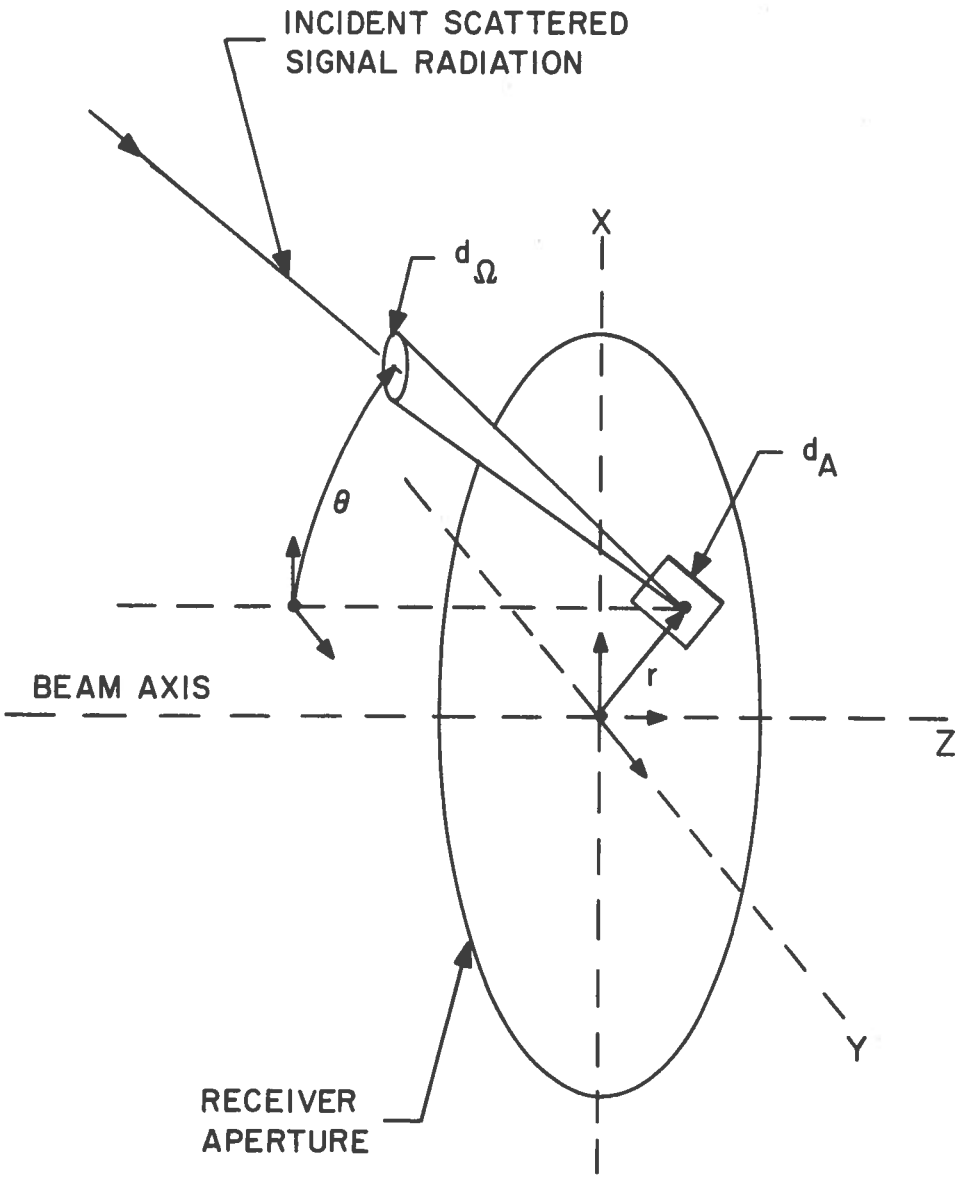

Figure 30. Nomenclature of Position and Angular Incidence of Radiation Reaching the Receiver Aperture Plane.

$$\sigma_\theta^2 = \gamma_f N_e \theta_1^2 + \sigma_{\theta o}^2$$

$$\sigma_r^2 = \tau^2 \sigma_\theta^2 / 3 + \sigma^2_{ro} \qquad (23)$$

$$= - 3/2$$

Here the following definitions and typical values for this experiment apply:

γ_f - forward scattering efficiency for single scattering, ~0.96,

N_e - link optical thickness expressed in scattering mean free paths, $\lesssim 10$.

θ_1 - r.m.s. single scatter angle for ambient aerosol, ~0.295 radians,

τ - physical beam length, 768 meters,

$\sigma_{\theta o}$ - angular beamwidth at the transmitter, $<0.5 \times 10^{-3}$,

σ_{ro} - spatial beamwidth at the transmitter, = .05m.

The intensity distribution of Equation (21) evaluated with the above parameter values can be inserted in Equation (22) to arrive at an expression for integrated signal power collected by an axially-centered receiver of aperture radius R and field of view half-angle θ. The result, which is valid for moderate optical thickness Ne is

$$P_r(R, \Theta) \simeq \frac{6 C_f R^2}{\tau^2 \sigma_\theta^2} \left(1 - \exp[-\Theta^2 / 2\sigma_\theta^2]\right),$$

$$P_D(R,\Theta) = e^{-N_e} C_R/\Omega_T, \quad C_R<\Omega_T$$

$$= e^{-N_e}, \quad C_R>\Omega_T \qquad (26)$$

where C_T, C_R, and Ω_T are link geometry parameters which were defined earlier. For the scattered signal component, the received power integral reduces to the approximate relation

$$P_S(R, \Theta) = \frac{6(1-e^{-N_e})e^{-(1-\gamma_f)N_s}}{0.0835N_S} \quad \frac{R^2}{\tau^2}$$

$$x(1-e^{-\Theta^2/0.167N_S}) \qquad (27)$$

The relative levels of received direct and scattered signal as a function of the transmitter/receiver optical thickness can be estimated using Equations (26) and (27). For our experimental communication link, typical values of the geometry parameters under fog conditions were $C_R = 7\pi \times 10^{-8}$, $C_T \approx 4.8\pi \times 10^{-6}$, and $\Omega_T \approx 2 \times 10^{-6}$. (The large value of C_T takes into account the significant image spreading of the receiving Fresnel lens.) The predicted relative direct and scattered signal levels are shown in Figure 31. The implication of the plotted direct and scattered power levels is that for line-of-sight optical links with transmitter/receiver separations of up to a few times the visual range, signal dispersion in time and frequency due to aerosol scattering can be made quite negligible. If communication must be conducted by scattered radiation alone, the available signal is generally several orders of magnitude less than the optimum line-of-sight signal.

4.2 FOG CHANNEL EXPERIMENTS

A field site at Otis Air Force Base in Cataumet, Massachusetts was chosen for these experiments for a number of reasons, including the usually high incidence of low visibility fog during the spring and fall seasons and the convenience of a fog forecasting capability at the base weather station. The experimental link was made operational by early spring 1971 in anticipation of several instances of optimum fog conditions. As it turned out, there developed during the season only two opportunities for conducting tests under heavy fog conditions, and the second of these occasions, when the greater part of our data was acquired, happened within only a few days of the formal end of the program. Despite the relatively little data available, there appear to be certain definite conclusions to be drawn, as will be discussed presently.

4.2.1 PULSE BROADENING MEASUREMENTS

Pulses generated in an He-Ne laser were transmitted over the 768 M test link and detected with various receiving optics/detector combinations. The laser was operated at an average output power of 40 milliwatts; the mode-locked pulses had roughly a 1 nanosecond width, a 75-MHz repetition rate, and thus a peak power of about 0.5 watt. The initially small (~3 cm diameter) laser beam was diverged to a diameter of about 1 m at the receiver. The receiving telescope consisted of a rectangular 40 cm x 55 cm, 74 cm focal length Fresnel objective lens with a variable iris aperture at the focal plane. Directly behind the iris, a 2 in. focal length condensing lens was placed so as to focus the Fresnel lens aperture on the detecting photocathode. Thus, the size of the photocathode determined the effective telescope aperture, and detection sensitivity was relatively uniform over the angular field of view. The iris provided a variable field of view of up to 2° half angle. The top half of this aperture was covered by a half-plane stop to exclude the image of possible scattered light from the ground. It was also fitted with a removable "beam stop" which excluded the central 0.25° of the field of view when in place. Because of the considerable scattering of light by the Fresnel lens, this beam stop failed to remove efficiently the direct beam energy. A measured profile of the apparent distribution of light from the laser when seen through the Fresnel lens in clear air is shown in Figure 32. From this we conclude that the stop effectively cut out about 90% of the direct beam.

The Fresnel lens telescope was used in conjunction with any of three photomultipliers: an RCA model 8645, an Ampex model XP1210, or a Sylvania model 502. While the RCA and Ampex

tubes provided more than 13 dB greater sensitivity than the Sylvania tube, their impulse response characteristics were inadequate for unequivocal detection of atmospheric pulse broadening. Thus the search for this effect was conducted primarily with the crossed-field Sylvania detector.

Using these fast response photodetectors at necessarily low signal levels, considerable detector quantum shot noise is encountered. The inherent average transmitted pulse information was recovered under these circumstances by using a computer-controlled sampling oscilloscope system for accumulation of pulse shape and pulse height distribution data over long trains of received pulses. The final pulse data are comprised of averages of pulse amplitude samples taken at a set of programmed discrete time delays synchronized with the controlling oscillator of the mode-locked laser. This system is described in detail in chapter 2 of this report.

Figure 33 shows typical data taken with the XP1210 photomultiplier and the Fresnel lens optics. The lower trace is a pulse shape measured on a clear day and the upper trace is a measurement taken in fog of moderate visibility (~0.78 miles). The relative gain of the two traces is 10:1, and both curves are drawn to the same indicated time scale. There is no evident change in pulse shape, albeit the 10.4 dB attenuation of the fog transmission.

Figure 34 shows typical data taken with the RCA 8645. The upper trace was obtained with a full 2° field of view; the lower trace is with the center of the field of view removed by the 0.25° stop. As in the foregoing case, the pulses show the characteristic impulse response of the tube rather than signs of true atmospheric broadening. The beam attenuation is estimated in each case to be more than 20 dB, though taking a corroborating clear air calibration was neglected by oversight.

That there is indeed no detectable pulse broadening at the fog densities observed in this experiment is best shown in the crossed field detector data. Figure 35 shows the measured shape of pulses propagated in clear air, and Figure 36 shows typical pulse traces obtained under moderate fog conditions with the Sylvania model 502 tube. The two larger pulse traces shown were taken with the full 2° field of view aperture. The lower trace was obtained with the beam stop in place. Again no pulse broadening is evident.

To lend more credence to the impression of the absence of broadening, even in the weakest received signals, all of the data taken with this tube are corrected for bias and replotted semi-logarithmically in Figures 37 and 38. The

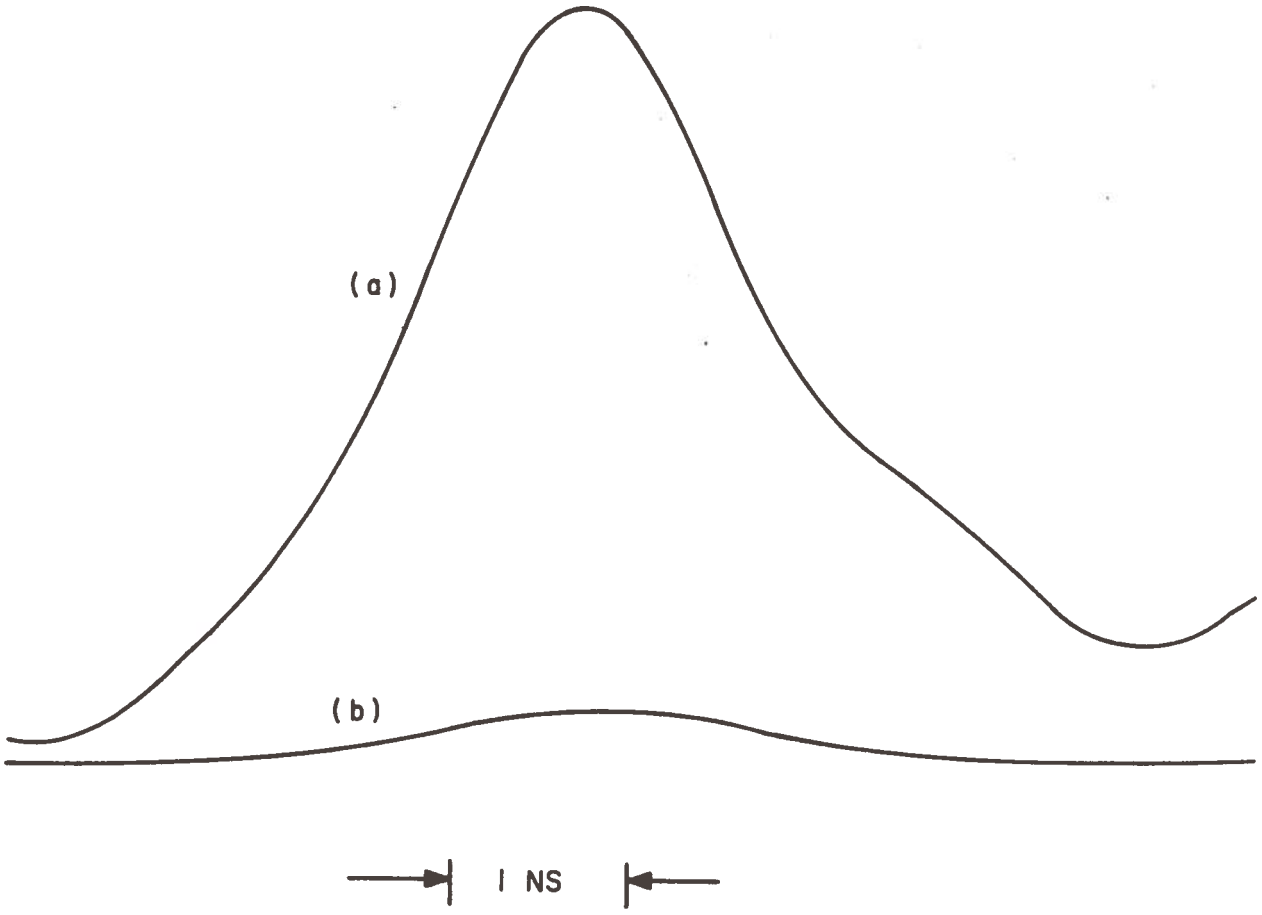

Figure 34. Typical Pulse Transmission Data taken with the RCA 8645 Photomultiplier, (a) Full Field of View, (b) Center of Field of View Excluded. Time Scale: 1 ns/div.

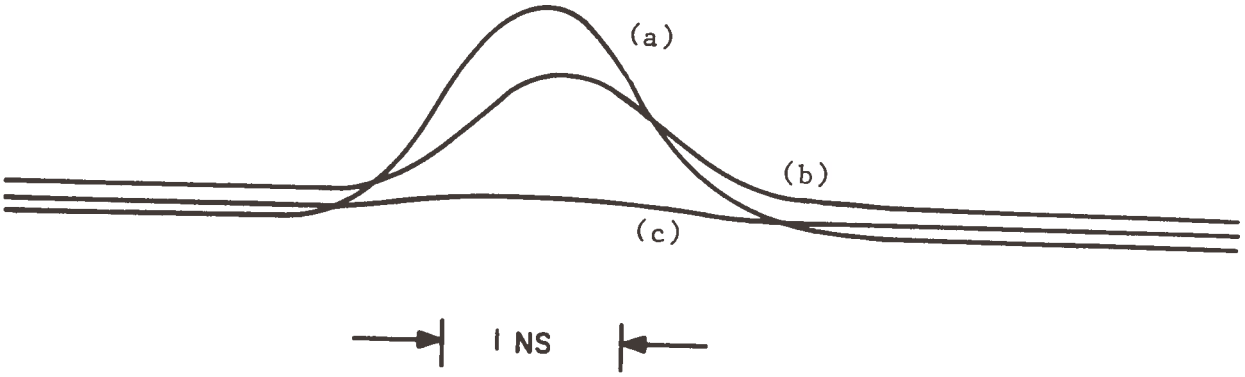

Figure 36. Pulse Shapes Measured Under Fog Conditions with Sylvania Crossed-field Detector. (a-b) Full Field of View Aperture, (c) Central 0.25° of Field of View Excluded. Beam Optical Thickness is ~ 2.0. Time Scale: 1 ns/div.

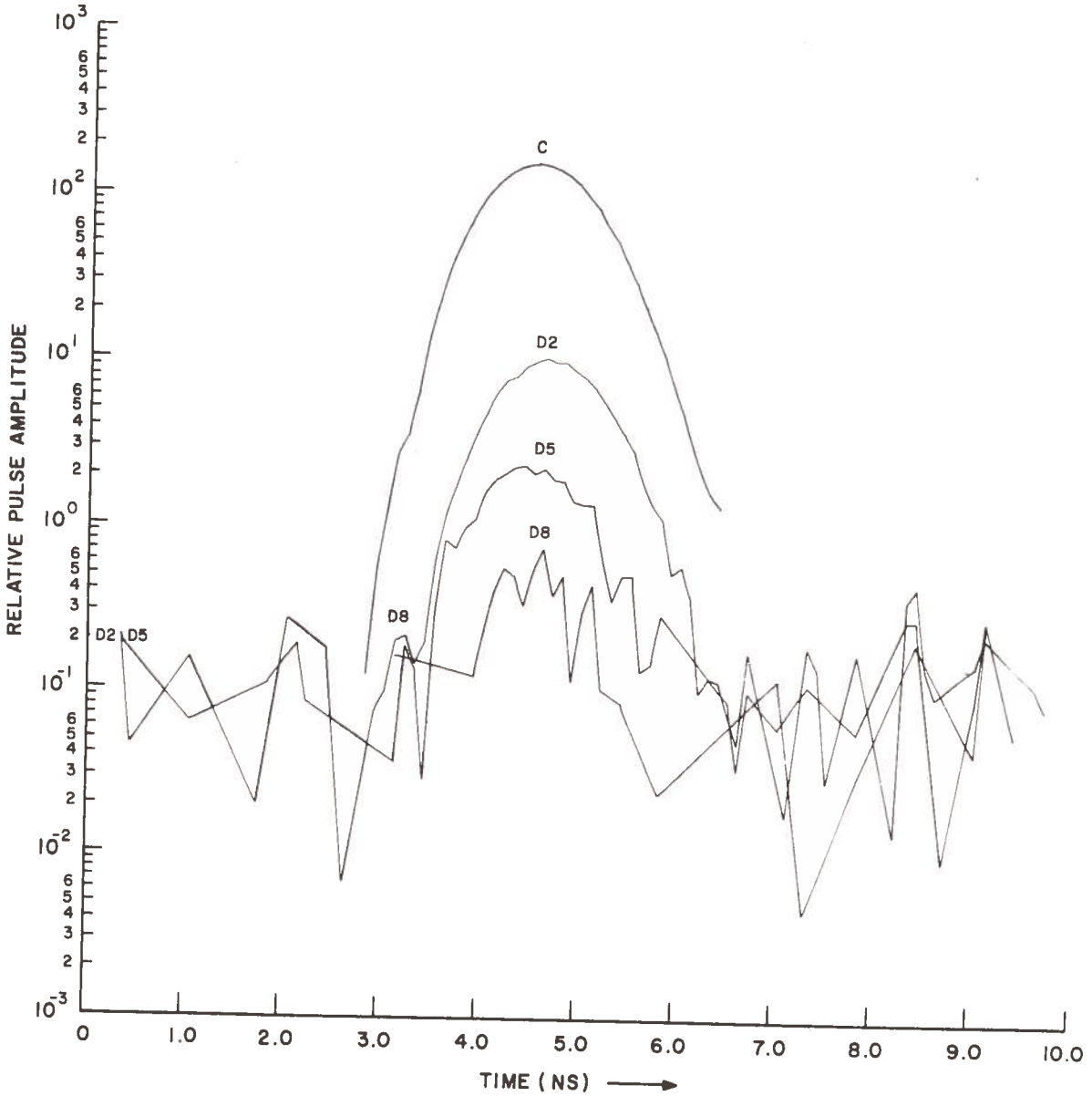

Figure 38. Semi-Logarithmic Plot of Pulse Shapes Observed Using Crossed-field Detector and Field of View with Central Beam Stop. Curve C is Clear Air Pulse, D2-D8 are for Fog Attenuated Pulses.

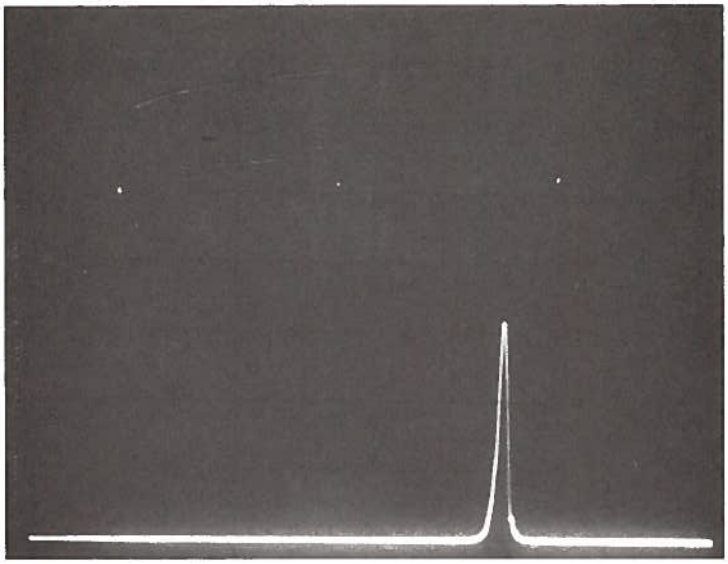

Figure 39. Oscilloscope Trace of Portion of Measured Frequency Spectrum of Laser Signal Transmitted Through Fog Near a Harmonic of the 75 MHz Pulse Repetition Frequency. Full Field of View Aperture and RCA 8645 Photomultiplier were Used.

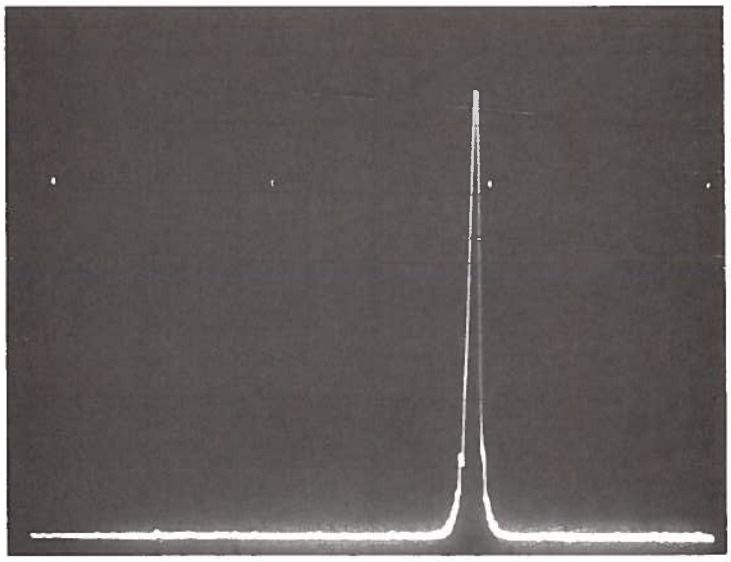

Figure 40. Oscilloscope Trace of Portion of Frequency Spectrum of Laser Signal Transmitted Through Fog. Signal Detected by RCA 8645 Photomultiplier with Center of Field of View Blocked.

The magnitudes of these measured scattering coefficients are also unexpectedly somewhat high, i.e.,~ 10^{-3} compared to an apparent extinction coefficient $\beta_e \sim 3 \times 10^{-5}$/cm (based on the pulse attenuation evident in the data of Figure 33). A problem apparent at the time of data taking was the high variability of the fog thickness and composition, which could be a partial explanation of the above discrepancies. Another unknown factor is the variation of the fog with height. However, there was no opportunity to carry out an intended arrangement elevating the nephelometer to the level of the laser beam. A corroboration of the data of Figure 41 might be obtained by a post experiment recalibration, but this will also not be undertaken for lack of time. Theory and procedure of calibration of the nephelometer are discussed elsewhere in this report (Section 2.9.4).

4.3 CONCLUSIONS

The original objective of these experiments was to delineate the characteristics of an optical communication channel operating in natural aerosol media (i.e., fog) as might frequently happen with unprotected atmospheric line-of-sight communication links. It was hypothesized that, since the angular scattering of optical radiation by typical natural aerosol particle distributions is strongly peaked in the forward direction, scattered light would constitute a significant source of transmitted signal energy over a link in a moderately thick scattering medium.

During the only two opportunities for observation of fog transmission, we were able to investigate a limited range of optical configurations which closely simulated a low power, line-of-sight communication link with certain features, e.g., a fairly well-directed beam and a moderately narrow receiving field of view (2°).

No complete analysis is available which predicts the time or frequency dispersion of such a link operating in fog. A simple consideration of a possible doubly scattered ray path (Figure 42) leads to an estimate of the typical relative delay of a multiply-scattered ray $\Delta t \sim L\theta^2/2c$, where θ is the angle of incidence of the final ray segment on the receiving aperture. For an angle of 2°, which is the limit of our field of view, this estimate is about 2.5 nanoseconds (L = 768 m). Significant amounts of scattered radiation (i.e., say 10% of the detected signal) arriving with such delays would surely have been observable with the crossed-field detector employed. We find however no

5. REFERENCES

Certain citations have document accession numbers given such as NXX-XXXXX; AXX-XXXXX. These indicate where abstracts, and in many cases the report or paper, can be obtained. The symbols are defined in Table 5-1 of Thompson (1971).

Brookner, E. (1970), Atmosphere propagation and communication channel model for laser wavelengths, IEEE Trans. Communication Technology, COM-18, 396-416

Bucher, E. A., R. M. Lerner, and C. W. Niessen (1970), Some experiments on the propagation of light pulses through clouds, Proc. IEEE, 58, 1564-1567.

Chandrasekhar, S. (1960), *Radiative Transfer*, Dover, New York.

Chu, T. S. and D. C. Hogg (1968), Effects of precipitation on propagation at 0.63, 3.5 and 10.6 microns, Bell System Technical J., 47, 723-761.

Clark, J. R. and S. Karp (1970), Approximations for lognormally fading optical signals, Proc. IEEE, 58, 1964-1965, reprinted in Chapter 6 of this report.

deWolf, D. A. (1968), Saturation of irradiance fluctuations due to turbulent atmosphere, J. Optical Society of America, 58, 461-466.

Fried, D. L. (1967A), Aperture averaging of scintillation, J. Optical Society of America, 57, 169-175.

Fried, D. L. (1967B), Propagation of a spherical wave in a turbulent medium, J. Optical Society of America, 57, 175-180.

Fried, D. L., Mevers, G. E. and M. P. Keister, Jr. (1967), Measurements of laser beam scintillation in the atmosphere pp. 247-292 in Theoretical Analysis of Atmospheric Effects on Optical Propagation, Final Report on Contract No. NAS8-18035, North American Aviation, Inc., Autonetics Div., Anaheim, CA.

Fried, D. L. and J. B. Seidman (1967), Laser-beam scintillation in the atmosphere, J. Optical Society of America, 57, 181-185.

Gilder, J. R. and K. Hao (1970), Experimental study of the transient response of multiple scattered laser radiation, Proc. IEEE, 58, 1764-1766.

Ochs, G. R. (1969), Measurement of 0.63 micron laser beam scintillation in strong atmospheric turbulence, Report No. ESSA-TR-ERL-154-WPL-10, ESSA Wave Propagation Laboratory, Boulder, CO, N70-36086#.

Ochs, G. R. and R. S. Lawrence (1969), Saturation of laser-beam scintillation under conditions of strong atmospheric turbulence, J. Optical Society of America, 59, 226-227, A69-22079#.

Middleton, D. (1960), *An Introduction to Statistical Communication Theory*, McGraw-Hill, New York.

Pritchard, B. S. and W. G. Elliott (1960), Two instruments for atmospheric optics measurements, J. Optical Society of America, 50, 191-202.

Rushforth, C. K. and R. W. Harris, (1968), Restoration, resolution, and noise, J. Optical Society of America, 58, 539-545.

Strohbehn, J. W. (1968A), Comments on Rytov's method, J. Optical Society of America, 58, 139-140

Strohbehn, J. W. (1968B), Line-of-sight propagation through the turbulent atmosphere, Proc. IEEE, 56, 1301-1318.

Tatarski, V. I. (1961), *Wave Propagation in a Turbulent Medium*, McGraw-Hill, New York, Reprinted by Dover, New York in 1967.

Thompson, W.I. III (1971), Atmospheric transmission handbook: A survey of electromagnetic wave transmission in the earth's atmosphere over the frequency (wavelength) range 3 kHz (100 km) - 3,000 THz (0.1 micron), Report No. DOT-TSC-NASA-71-6, DOT/Transportation Systems Center, Cambridge, MA, N71-20121#.

6. SELECTED REPRINTS

Reprinted from the PROCEEDINGS OF THE IEEE
VOL. 58, NO. 10, OCTOBER, 1970
pp. 1611–1626

Communication Theory for the Free-Space Optical Channel

S. KARP, MEMBER, IEEE, E. L. O'NEILL, AND R. M. GAGLIARDI, MEMBER, IEEE

Abstract—The current understanding of quantum detectors, the noise mechanisms which limit (are basic to) their operation, and their application to optical communications (theory) is summarized. In this context, we are considering channels in which the electromagnetic field is not subjected to any propagation effects other than a geometric loss. (Such a channel would exist between satellites.) Consequently, we will concentrate on optimum time processing using the tools of statistical communication theory.

Fundamental to the study of a detection process is the need to develop a good mathematical model to describe it [1]–[6]. Therefore, approximately one-fifth of the paper is devoted to establishing, in a semi-classical analysis, the quantum detector output electron number as a conditional Poisson process with the conditioning variable being the modulus of the electromagnetic field. Once this has been established, these results are used to derive various limiting probability densities related to actual practice. Although the mathematical details are omitted, these results will be presented from the viewpoint of orthogonal function expansions and interpreted in terms of an eigenspace.

The resulting current flow is analyzed next as a shot noise process, and the power density spectrum is calculated. Attention is focused on isolating the signal components from the noise in terms of both the current probability density and the power density spectrum. Examples are given where appropriate. At this point, an understanding of the underlying noise processes will have been presented and attention will shift to analog and digital communications.

The analog communication will be presented primarily in terms of the signal-to-noise ratio. The *S/N* ratio in direct detection will be presented both as a ratio of the integrals of two separate portions of the spectrum and as a ratio of two moments of the probability density describing the current. These calculations will be extended to include heterodyne detection.

Digital communications will be discussed in the context of detection theory. It will be shown that the likelihood ratio is often a monotonic function of the random variable representing the number of electrons flowing. Hence optimum processing will consist of a weighted count of electrons from various counting modes. Digital design will be presented in terms of *M*-ary signaling, error probabilities, and information rates.

Manuscript received May 15, 1970.

S. Karp was with the NASA Electronics Research Center, Cambridge, Mass. He is now with DOT Transportation Systems Center, Cambridge, Mass.

E. L. O'Neill is with the Worcester Polytechnic Institute, Worcester, Mass.

R. M. Gagliardi is with the University of Southern California, Los Angeles, Calif.

I. INTRODUCTION

WE BEGIN with a classical description for the energy and momentum densities of a radiation field for both the single- and multimode cases. Confining our treatment to the semi-classical theory, we sketch briefly the argument that the probability of ejecting an electron from a photo-cathode surface in a short time interval is proportional to the light intensity. From this point of view, we deduce an expression for the probability of releasing n photoelectrons in a time T in terms of a weighted Poisson distribution. The weight factor is the probability distribution for the accumulated energy received on the photodetective surface in equal times.

A. Semi-Classical Theory

1) Normal Mode Decomposition of the Field: We begin our description of the semi-classical theory of radiation and matter by writing down the free space wave equation for the vector potential $\vec{A}(\vec{r}, t)$

$$\nabla^2 \vec{A} - \frac{1}{c^2} \frac{\partial^2 \vec{A}}{\partial t^2} = 0. \tag{1}$$

$$\vec{G} = \sum_{l,\sigma}\sum \frac{2\varepsilon_0 V\omega_l^2}{c} a_{l\sigma}^* a_{l\sigma}\hat{k}_l = \sum_{l,\sigma}\sum \frac{H_{l\sigma}}{c}\hat{k}_l. \tag{13}$$

These equations indicate that so far as energy and momentum are concerned, the radiation field may be considered as a collection of oscillators, each contributing (per mode) to the total energy and momentum. We point out here that a quantum oscillator's level of excitation is given by $H_{l\sigma} = n_{l\sigma}\hbar\omega_l$ and when this condition is inserted into (13) there results the conclusion that a radiation field may be treated as a superposition of discrete photons, $n_{l\sigma}$ per mode, each possessing energy $\hbar\omega_l$ momentum $\hbar\omega_l/c$ and angular momentum $\pm\hbar$.

2) Interaction Between an Atom and a Radiation Field: A complete description of the emission and absorption of light by an atom influenced by a radiation field is well beyond the scope of this paper. The reader, interested in the details of the process, is urged to consult [7]–[10]. We present here only a bare outline of the approach insofar as it related to the photon counting distribution.

Starting with the complete Hamiltonian for a charged particle in an electromagnetic field

$$H = \frac{(\vec{p} - e\vec{A})^2}{2m} + H_R + eV \tag{14}$$

we neglect the term in e^2 and use the gauge condition div $A = 0$ to reduce this to

$$H = H_A + H_R + H_I \tag{15}$$

where $H_A = (p^2/2m) + eV$ is the Hamiltonian of the atom,

$$H_R = \sum_l \sum_\sigma H_{l\sigma}$$

is the Hamiltonian of the radiation field, and $H_I = -(e/m)\vec{A}\cdot\vec{p}$ is the interaction Hamiltonian. Combining the first two terms into the unperturbed Hamiltonian $H_0 = H_A + H_R$, we next treat H_I as a perturbation and attempt to solve the Schrödinger equation

$$(H_0 + H_I)|\psi\rangle = i\hbar\frac{\partial|\psi\rangle}{\partial t}. \tag{16}$$

Using the method of first order perturbation theory, we attempt an expansion of $|\psi\rangle$ into a linear combination (with time varying coefficients) of the eigenstate $|\psi_n^0\rangle$ of the unperturbed Hamiltonian, known to satisfy the equation

$$H_0|\psi_n^0\rangle = i\hbar\frac{\partial|\psi_n^0\rangle}{\partial t}. \tag{17}$$

In this expansion we have

$$|\psi\rangle = \sum_n C_n(t)\exp\left(-\frac{i}{\hbar}E_n t\right)|\psi_n^0\rangle \tag{18}$$

and the probability of finding the system in a state $|\psi_n^0\rangle$ is

$$|C_n(t)|^2 = |\langle\psi_n^0|\psi\rangle|^2. \tag{19}$$

Assuming then that the combined system, atom plus radiation field, begins in some initial state, $|i\rangle$, (18) implies a set of coupled equations for the probability amplitude ($C_n(t)$) from which one can determine $|C_f(t)|^2$, the probability of finding the combined system in the final state $|f\rangle$. Summing over all final states, and making a number of simplifying assumptions [8]–[10], one ends up with Fermi's "golden rule" for the probability per second for a transition in the form

$$\frac{dP}{dt} \cong \frac{2\pi}{\hbar}|\langle f|H_I|i\rangle|^2\rho(E_f). \tag{20}$$

Here $\rho(E_f)$ is the density-in-energy of the final states, and $\langle f|H_I|i\rangle$ represents the matrix element of the perturbation Hamiltonian between the initial and final states. When applied to the problem of an atom in a radiation field, one must distinguish between the cases when only the atom and both the atom and the radiation field are treated as quantized systems. In the former, the semi-classical treatment, one can correctly deduce Einstein's B coefficient for stimulated emission and absorption in terms of the electric dipole moment taken between the initial and final wave functions of the atom. On the other hand, when one also quantizes the field including the zero point fluctuation, then (20) also predicts the existence of Einstein's A coefficient for spontaneous emission.

3) Photon Counting Statistics: The consequence of (20) that is of importance to us is that it leads [8] to the result that in a short time Δt the probability of ejecting an electron from an atom on the surface of a photocathode is proportional to the incident intensity of the light $I(t)$. That is

$$P_1(t, t + \Delta t) = \alpha I(t)\,\Delta t. \tag{21}$$

For sufficiently short times $P_0(t, t+\Delta t) \cong 1 - \alpha I(t)\,\Delta t$ so that in an interval $(0, t + \Delta t)$ there are but two ways of releasing n photo-electrons, given by

$$P_n(0, t + \Delta t) = P_{n-1}(0, t)\alpha I(t)\Delta t + P_n(0, t)(1 - \alpha I(t)\Delta t). \tag{22}$$

Subtracting $P_n(0, t)$ from both sides and dividing by Δt before passing to the limit, we can write

$$\frac{dP_n}{dt} = \alpha I(t)P_{n-1}(t) - \alpha I(t)P_n(t). \tag{23}$$

The solution to this differential-difference equation is

$$P_n(t) = \frac{\left[\alpha\int_0^t I(t')\,dt'\right]^n \exp\left[-\alpha\int_0^t I(t')\,dt'\right]}{n!}. \tag{24}$$

Now if this process were carried out a number of times over similarly prepared realizations of the field, the average over this ensemble would lead to

$$P_n(t, T) = \int_0^\infty \frac{(\alpha w)^n \exp(-\alpha w)}{n!} P(w)\,dw \tag{25}$$

where

$$w = \int_t^{t+T} I(t')\,dt'$$

and $P(w)dw$ is the probability for w to lie in the range $(w, w+dw)$.

1) The $\{\phi_i(\tau)\}$ are solutions to the integral equation

$$\lambda_i\phi_i(\mu) = \int_0^t K_n(\mu, v)\phi_i(v)\,dv$$

where

$$K_n(\mu, v) = E[n(\mu)n^*(v)]$$

in the covariance function of the noise and is a real function.

2) $a_i(\sigma)=\int_0^t a(\tau, \sigma)\phi_i^*(\tau)\,d\tau=(a, \phi_i)=(s, \phi_i)+(n, \phi_i)$.

3) The equality is in the sense of "limit-in-the-mean."

4) $(\phi_i, \phi_j)=\delta_{ij}$

5) The $a_i(\sigma)$ are independent Gaussian random variables, when conditioned on σ.

The generating function of this process N_t can then be written as [12]

$$M_{N_t}(s) = E\left[\exp\left(\alpha\int_0^t |a(t, \sigma)|^2 dt[e^\mu - 1]\right)\right]$$
$$= E\left[\exp\left(\alpha\sum_{i=0}^{\infty} |a_i(\sigma)|^2(e^\mu - 1)\right)\right]$$

which, using property (5) and [13] reduces to

$$M_{N_t}(s) = \prod_{i=0}^{\infty} E[\exp(\alpha|a_i(\sigma)|^2[e^\mu - 1])]$$
$$= \prod_{i=0}^{\infty} \frac{\exp(\alpha|s_i(\sigma)|^2(e^\mu - 1)/[1 - \alpha\lambda_i(e^\mu - 1)])}{1 - \alpha\lambda_i(e^\mu - 1)}. \quad (36)$$

At this point, the variable σ will be suppressed, although it must be considered as a conditioning variable when encountered in practice.

Notice that $M_{N_t}(s)$ is a product of similarly distributed functions. The inverse transform of the ith component is

$$P_{N_{t_i}}(k_i) = \frac{(\alpha\lambda_i)^{k_i}}{(1 + \alpha\lambda_i)^{1+k_i}}\exp\left(\frac{-\alpha|s_i|^2}{1 + \alpha\lambda_i}\right)L_{k_i}\left(\frac{-\alpha|s_i|^2}{\alpha\lambda_i(1 + \alpha\lambda_i)}\right) \quad (37)$$

where $L_x(y)$ is the Laguerre polynomial.

1) No Additive Noise: In the limit as $\lambda_i\to 0$ (37) approaches

$$\lim_{\lambda_i\to 0} P_{N_{t_i}}(k_i) = \frac{[\alpha|s_i|^2]^{k_i}}{k_i!}\exp(-\alpha|s_i|^2)$$

and

$$P_{N_t}(k) = \frac{\left[\alpha\sum_{i=0}^{\infty}|s_i|^2\right]^k}{k!}\exp\left(-\alpha\sum_{i=0}^{\infty}|s_i|^2\right)$$
$$= \frac{(\alpha E_S)^k}{k!}\exp(-\alpha E_S) \quad (38)$$

where $k=\sum_{i=0}^{\infty} k_i$ is the total count and $E_S=\sum_{i=0}^{\infty}|s_i|^2$ is the total signal energy in the $(0, t)$ interval. Thus the deterministic signal alone yields a Poisson distributed count. This, of course, could have been deduced immediately from (34). Notice, however, that when $|s_i|^2=0$

$$P_{N_{t_i}}(k_i) = \frac{(\alpha\lambda_i)^{k_i}}{(1 + \alpha\lambda_i)^{1+k_i}} \quad (39)$$

and each of the coordinate components is Bose-Einstein distributed [4].

In summary we see that: the signal alone can be considered to be Poisson distributed along each of its coordinate axes in Hilbert Space; Gaussian noise alone is Bose-Einstein distributed along a particular set of coordinate axes in Hilbert Space; when signal is added to the noise the resultant process is distributed according to (37) along each of the coordinate axes determined by the noise alone.

2) Band-Limited White Gaussian Noise: An important case occurs in communication theory when the signal and noise are passed through a filter before detection. We will consider the case where the process $a(\tau)$ is band limited by a rectangular filter with bandwidth $2B$. We will also assume that the noise was initially white, with spectral density N_0.

It has been shown [14] that when a process is band limited and then observed over a time interval $(0, t)$ the eigenfunctions are prolate spheroidal wavefunctions. It has also been shown that the first $(2Bt+1)$ of these functions accurately approximate the original function. This appears valid for values of $2Bt$ as low as 3 and 5 [11]. Therefore, it is a good engineering approximation to assume that the eigenvalues associated with the first $(2Bt+1)$ coordinates are each N_0 with the remaining ones being zero. The generating function $M_{N_t}(s)$ in (3) then becomes

$$M_{N_t}(s) \simeq \frac{\exp\left[\dfrac{\alpha(s, s)(e^\mu - 1)}{1 - \alpha N_0(e^\mu - 1)}\right]}{[1 - \alpha N_0(e^\mu - 1)]^{2Bt+1}} \quad (40)$$

with the corresponding probability density being

$$P_{N_t}(k) = \frac{(\alpha N_0)^k}{(1 + \alpha N_0)^{k+2Bt+1}}$$
$$\cdot\exp\left[\frac{-\alpha(s, s)}{1 + \alpha N_0}\right]L_k^{2Bt}\left[\frac{-\alpha(s, s)}{\alpha N_0(1 + \alpha N_0)}\right] \quad (41)$$

where $L_k^{2Bt}(x)$ is the Laguerre polynomial. We will now consider some limiting forms of (41).

3) No Signal: In the absence of signal, (41) reduces to

$$P_{N_t}(k) = \binom{2Bt + k}{k}\left(\frac{1}{1 + \alpha N_0}\right)^{2Bt+1}\left(\frac{\alpha N_0}{1 + \alpha N_0}\right)^k$$

which is a negative binomial distribution. There are two important limiting cases for this distribution.

a) Limit $2Bt \to 0$

$$P_{N_t}(k) = \frac{(\alpha N_0)^k}{(1 + \alpha N_0)^{k+1}}.$$

For $2Bt \ll 1$, there is only one significant eigenvalue, the average value. Since this occurs when $t \ll 1/2B$, it can clearly be related to the approximation

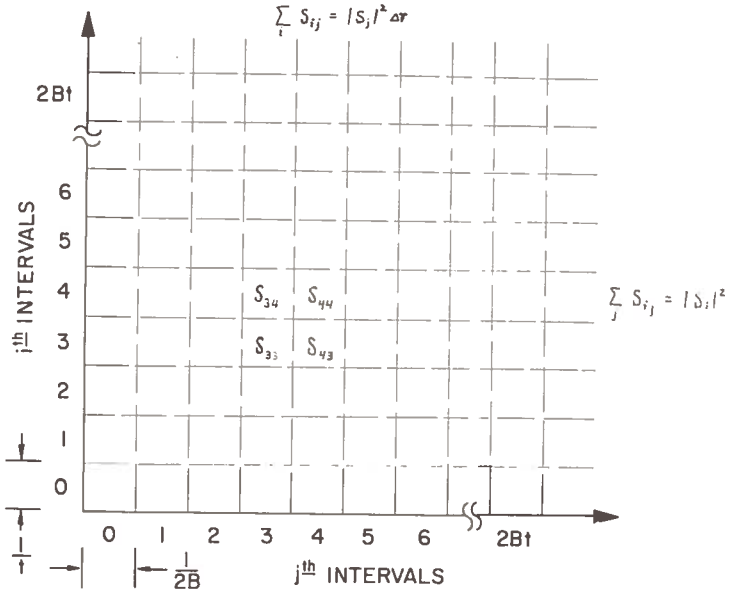

Fig. 1. Time-frequency representation in terms of $i-j$ intervals.

band $(-B+i/t, -B+(i+1)/t)$ for a time t. The first measurement is a sum of all the squares in the jth column, while the latter is a sum of all the squares in the ith row.

If the process is not wide sense stationary, we can still use Parseval's Theorem to write (s, s) as

$$(s,s) = \int_0^\infty P(f)\,df \simeq \sum_{l=0}^{2Bt} P(l\Delta f)\Delta f$$

and write a density similar to (44). K_l would be the total count in the band Δf in the interval $(0, t)$. However, one cannot assign the rigorous definition of power density spectrum to the noise and the noise coefficients.

We note, finally, that the most common statistical behavior encountered in practice yields $2B\Delta T \gg 1$. Hence condition 4b) applies to any measurement interval of length ΔT. Thus the observance of counts over many independent ΔT intervals is a sum of independent Poisson variables. This interpretation was first proposed by Reiffen and Sherman [17] on the heuristic basis, but can clearly be shown to have a solid foundation.

III. Shot Noise Processes

We have shown that a linear relation exists between the average power I of the radiation (over some finite aperture) and the rate of flow of photons n. Thus if n is a function of time, we can write

$$I(t) = h\nu n(t) \tag{45}$$

where h is Planck's constant and ν is the photon frequency. Thus the detector of optical radiation can be represented either as an instantaneous power detector or as an instantaneous rate detector. This relationship is generally explained by postulating that each incident particle independently releases an electron with probability η upon arrival at the photodetector surface, the electron in turn traveling to a cathode surface yielding a current "impulse" effect at the detector output. Thus the total output current $i(t)$ is due to the motion of a collection of electrons, proportional in number to the arriving particles. We can, therefore, write for the output current flow $i(t)$

$$i(t) = \sum_{m=1}^{N_t} h(t - t_m) \tag{46}$$

where $h(t)$ is the current impulse effect, t_m is the time of release of the mth photoelectron, and N_t is the number of such electrons occurring in the total time interval $(-\infty, t)$. The function $h(t)$ has area equal to the charge of an electron, while N_t is the counting statistic, discussed in Section II, of the photoelectron emissions. Note that if we neglect space-charge effects in the photodetector, the travel time of each released photoelectron is finite, which means that the function $h(t)$ must be time limited to some interval τ. That is, $h(t)=0$ for $t<0$ and $t>\tau$. In this case, N_t becomes the counting statistic over the finite interval $(t-\tau, t)$. Since τ is inversely related to the detector bandwidth, τ is relatively short ($10^{-10}-10^{-7}$ s), and can be considered a "delta function" with respect to most modulation waveforms. It perhaps should be pointed out that if $h(t)$ is assumed to be a flat rectangular function over $(0, \tau)$, then $i(t)=N_t-N_{t-\tau}$ and the detector output is precisely the counting process of the received optical radiation. If, instead, a nonrectangular impulse waveshape is to be accounted for, then one is forced into a closer examination of the processes described by (46). This class of processes can loosely be defined as "shot noise" processes (although the exact definition of the latter tends to vary in the literature).

function of the intensity process N at any time t. Thus the effect of the function G is to cause a departure of the first-order probability density of $i(t)$ from that of $n(t)$. The conditions under which the latter effect is negligible, and the shot noise process has approximately the first order density of N, have been studied by Karp and Gagliardi [26]. In this latter instance, we can say that the shot noise represents (statistically) the intensity process. This representation can be related to the "denseness" of the photon arrivals; i.e., the average number of photons per second. In fact, when the latter parameter is large, it can be shown that the bracketed term in (52) is approximately the characteristic function of a Gaussian random variable, with mean $n(t)$ and variance $n(t)$. This infers that the conditional (on N) probability density of $i(t)$ at any t approaches asymptotically a Gaussian density, which again may be loosely interpreted as an instantaneous "signal" $n(t)$, immersed in additive nonstationary Gaussian noise of variance $n(t)$.

The relation between shot noise and its intensity can be further investigated by consideration of the individual moments of the two processes. The moments of the process $i(t)$ can be obtained from its semi-invariants, which are, for PSN processes

$$\lambda_n(t) = \int_{t-\tau}^{t} h^n(t-\rho)n(\rho)\,d\rho. \tag{53}$$

The moments can then be obtained by the sequence of relations $E(i)=\lambda_1$, $E(i^2)=\lambda_2+\lambda_1^2$, $E(i^3)=\lambda_3+\lambda_1\lambda_2+\lambda_1^3$, etc. For conditional PSN processes, the λ_n are themselves random processes, and the moments of $i(t)$ depend upon the higher order moments of the process $n(t)$. However, if the intensities are continuous, or if the detector bandwidth is much larger than the bandwidth of the intensities, the rth moments are related by

$$E(i^r) = E(N^r) + D(r) \tag{54}$$

where $D(1)=0$ and $D(r)$, $r>2$, is function depending upon the higher order statistics of $n(t)$ and upon the function $h(t)$. This relationship was investigated in [26]. It was shown, for example, that if the function $h(t)$ was rectangular over $(0, \tau)$ the rth moment of $i(t)$ was approximately equal to the rth moment of the intensity process N if

$$\begin{bmatrix}\text{average number of}\\ \text{photon arrivals in}\\ \tau \text{ seconds}\end{bmatrix} \gg \frac{r(r-1)}{2}. \tag{55}$$

Equation (55) essentially states that the denseness of the shot events (i.e., the average number of $h(t)$ functions overlapping the time interval of one function) must be sufficiently large for moment representation. The right side of (55) serves as a rough rule of thumb for determining how large this denseness must be for approximate equality of the rth moment. It may be recalled [20] that for PSN processes (deterministic intensities) a condition of large number of shot occurrences is required before the PSN loses its discrete nature. Equation (55) can therefore be interpreted as the statistical equivalent of this statement; i.e., the condition under which the conditional PSN begins to take on the statistics of its intensity.

By using (54), it is also possible to relate the fluctuations in the detector output $i(t)$ to those of the intensity $n(t)$. Specifically, if we define the signal-to-noise ratio (SNR) of a positive process as the ratio of its mean value squared to the variance, then (54) leads to the fact

$$\text{SNR of } i(t) \leq \text{SNR of } n(t) \tag{56}$$

which implies that the percent fluctuations in the shot noise are always at least as great as those of the intensity itself. We make this point mainly because the foregoing definition of SNR is commonly used in assessing signal quality in communication system analysis.

It may be noted that the conditions for which the intensity is represented by a shot noise process are also useful in "building up" intensity models as shot noise. This type of shot noise modeling has been used for studying radiation scattering and perturbation effects [27], [28] in which the impulse functions $h(t)$ were reinterpreted as wave packets.

With the statistics of the conditional shot noise process identified (at least in first- and second-order statistics), the problem of optimal processing procedures at the photodetector output can now be properly formulated, and in some instances, solved. For example, the problem of optimal linear filtering of the process $i(t)$, so as to minimize the mean squared error from the desired intensity, was considered in [26]. For certain types of pulsed intensities, as in PCM communications optimal operations maximizing output signal to noise ratios have also been considered [29]. The application of estimation theory [30], tracking operations [31], and detection procedures [17], [18], [20] to the photodetector shot noise output has been under study, and appears to be a problem area of considerable interest from both a practical and theoretical point of view.

IV. Digital Communications and Optical Systems

The availability of an easily generated extremely narrow pulse in the optical region of the spectrum suggests a natural application to communication by digital methods. This notion, in turn, has fostered an increasing interest in the application of both classical detection theory and information to optical systems. Since the output of a photodetector is a sequence of electron counts, the detection problem is formally one of decisioning in the presence of generalized Poisson statistics. While early approaches to the problem basically were confined to pure Poisson counting [32], [33], more recent attention has included the generalized Laguerre counting processes in Section III, [13].

The formulation of the general M-ary detection problem involving counting statistics proceeds as follows. The transmitter sends a signal whose intensity is modulated with one of a set of M possible intensities, each T seconds long. The received signal is corrupted by background radiation, which we assume here is white Gaussian noise of level N_0 watts per hertz per unit area, and optical bandwidth B. The output of the photodetector at the receiver is then a

$\gtrless L_{k_i}^{x}(N/N_0)$ which, in turn, is true if $k_q \gtrless k_i$. Hence the maximum likelihood test need only count over each interval, selecting the signal corresponding to the interval with the largest count.

A. Error Probabilities with Pulsed Intensity Sets and Poisson Counting

The performance of the pulsed intensity set in M-ary detection can be evaluated by considering the error probability when Poisson counting statistics are assumed. This can be obtained by noting that for the pulsed intensity set of (60) the log of the likelihood functions for each k_i constitutes a set of independent Poisson random variables. The variable for k_q has intensity $(N+2B\alpha N_0\Delta T)$ if the qth intensity was sent, and has intensity $K=2B\alpha N_0\Delta T$ otherwise. Recall that if the qth intensity is sent a correct decision will be made with probability $1/(r+1)$ of the log likelihood equals r others and exceeds the remaining $M-(r+1)$. Therefore, upon considering all possibilities, the error probability can be derived as [20]

$$P_E(E, K, M) = 1 - \frac{e^{-(N+MK)}}{M} - \sum_{x=1}^{\infty}\left[\frac{(N+K)^x e^{-(N+K)}}{x!}\right] \cdot \left[\sum_{t=0}^{x-1}\frac{K^t e^{-K}}{t!}\right]^{M-1} \cdot \left[\frac{(1+a)^M - 1}{aM}\right] \quad (62)$$

where:

$$a = \left[\frac{K^x}{x!\sum_{t=0}^{x-1}\frac{K^t}{t!}}\right].$$

The function $P_E(N, K, M)$ has been plotted by Pratt [32] for $M=2$, and recently a digital computation has been generated [23] for a complete plot of the function. An exemplary plot is shown in Fig. 2 in which $P_E(N, 3, M)$ is plotted for various M as a function of N. It is important to note that P_E depends on both the normalized signal energy N and the normalized noise energy K in the counting interval, and not simply on their ratio. This fact is emphasized in Fig. 3, in which $P_E(N, K, 2)$ is plotted as a function of K for 2 fixed ratios N/K. This dependence on both signal and noise energies distinguishes the Poisson detection problem from the analogous coherent Gaussian channel problem. Note that the interfering noise energy K depends only upon the background energy in the interval ΔT, which is the width of the transmitted intensity pulse. The prime advantage of Poisson systems is precisely their ability to remove the effect of background noise by making ΔT small, and has been emphasized in previous reportings [36], [37].

The actual dependence of P_E on the parameter ΔT has been considered [38], and the improvement in error probability with decreasing ΔT has been demonstrated. The improvement, of course, is made at the expense of information bandwidth and peak power, both inversely proportional to ΔT. Surprisingly, the improvement is quite small at low values of N, and the increase in bandwidth may not be worth the decrease obtained in error probability. The effect

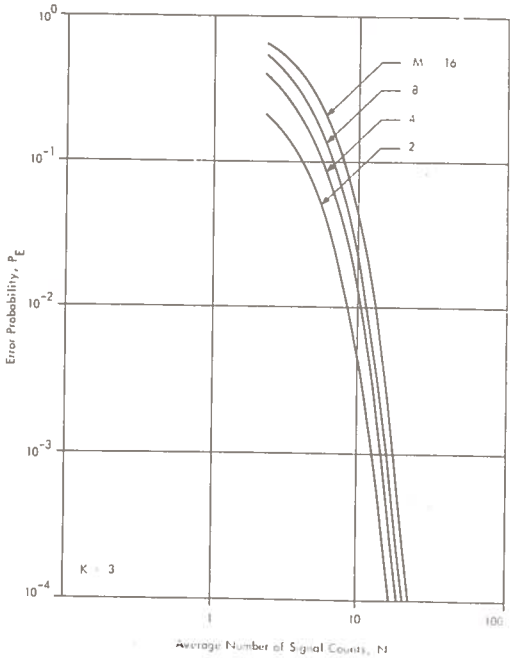

Fig. 2. Error probabilities for M-ary signaling.

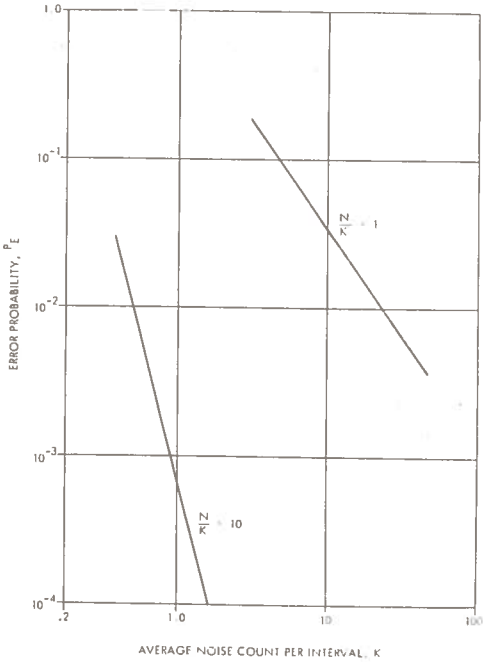

Fig. 3. Error dependence on signal and noise energies.

on error probability of additive extraneous thermal noise in the decisioning system and statistical characteristics of photomultipliers has also been considered [38].

For Laguerre counts, (62) must be rederived using the Laguerre densities discussed in Section III. Recently, general

width approaches the optical bandwidth) and the effect of additive noise can be accounted for by modifying these Poisson results [40].

The extension of the discrete model for optical detection (which was assumed almost entirely in the aforementioned references) to the continuous model has received little attention. In usual procedures, the continuous case is generated from the discrete by taking limits of infinitely small intervals. Although this procedure can be properly structured to generate the continuous version of the counting process, the continuous process representing the photodetector output must be viewed entirely as a shot noise process (see Section III). Unfortunately, such processes have first-order densities that are expressible only through transforms of their characteristic function. Hence the building up of a general detection model based upon shot noise rather than discrete processes would be severely hampered by the inability to express observable statistics. It would appear, however, that shot noise detectability cannot continue to be avoided when consideration is given to operation with information bandwidths on the order of optical detector bandwidths. This aspect of detection deserves more attention in future research studies.

V. Analog Communications

The major portion of work in the area of analog communications for optical systems has centered on first- and second-moment theory, spectral analysis, and signal-to-noise ratios. We have already discussed spectral analysis for shot noise processes with emphasis on signal representation. For the remainder of the paper we will concentrate on trying to bring together some of these ideas in a unified way, leaning heavily on physical motivation.

Before turning to the analyses required it is very instructive to reconsider the behavior of a photodetector from a phenomenological point of view. As we have already seen an important parameter in a photodetector is the time ΔT over which the intensity fluctuations remain relatively constant. This is related to the bandwidth B of the optical signal by $\Delta T \leq 1/2B$. When an electron is released from the detecting surface and flows through the ensuing circuitry, there is always the fixed electron charge e. This fixes the area of the resulting current pulse. Hence higher energy electrons will flow faster, the current pulses will be narrower in time resulting in an increased frequency response of the detector.

Generally, one thinks of counting circuitry as literally counting each of these events. On the other hand, one can also consider the following viewpoint: suppose we "match" the detector response B_d to the incident radiation bandwidth $\Delta T \simeq 1/2B = 1/2B_d$. Then each current pulse created will be approximately ΔT seconds wide. Hence at any time t, the effects of all pulses from the previous ΔT seconds will still be present. Therefore, if k_i electrons flow in the interval $(t_i - \Delta T, t_i)$, then at the time t_i the value of the current can be approximated by $k_i(e/\Delta T)$, or since $k_i/\Delta T \simeq \alpha \tilde{I}(t_i)$, $i(t_i) \simeq \alpha e \tilde{I}(t_i)$, which was shown earlier. If the response of the detector were square pulses, this description would be exact. On the other hand, the distortions occurring due to end effects are the normal effects of filtering. The so-called shot noise represents the fact that K_i is an integer, making $\tilde{I}(t_i)$ take on discrete values, whereas the true $I(t)$ would be continuous.

The previous argument was intended to justify consideration of the $(2Bt+1)$ Nyquist samples for analog processes also. It was shown in (55) that these samples can also be considered statistically independent.

1) *Maximizing Signal-to-Noise Ratio for Direct Detection:* For maximum likelihood detection, the optimum form of processing consisted of weighting the counts on each of the $(2Bt+1)$ intervals. We will, therefore, consider the form of processing where each k_j is weighted by the number β_j. The processed signal then becomes v, where

$$v = \sum_{j=0}^{2Bt} \beta_j K_j. \tag{67}$$

As a criterion for signal processing, we will use the signal-to-noise ratio defined as

$$\frac{S}{N} = \frac{E^2[v]|_{N_0}}{\operatorname{var}[v]} = 0. \tag{68}$$

Thus the mean of v in the absence of noise can be obtained from (37) and is

$$E[v]|_{N_0=0} = \alpha \sum_{j=0}^{2Bt} \beta_j |s_j(j\Delta T)|^2 \Delta T \tag{69}$$

with the variance being

$$\operatorname{var}[v] = \alpha \sum_{j=0}^{2Bt} \beta_j^2 \{(|s_j(j\Delta T)|^2 + N_0') + \alpha(N_0'^2 + 2N_0'|s_j(j\Delta T)|^2)\Delta T\}\Delta T \tag{70}$$

and $N_0' = N_0/\Delta T$.

Thus the signal-to-noise ratio becomes

$$\frac{S}{N} = \frac{\left\{\alpha \sum_{j=0}^{2Bt} \beta_j |s_j(j\Delta T)|^2 \Delta T\right\}^2}{\alpha \sum_{j=0}^{2Bt} \beta_j^2 \{(|s_j(j\Delta T)|^2 + N_0') + \alpha(N_0'^2 + 2N_0'|s_j(j\Delta T)|^2)\Delta T\}\Delta T} \tag{71}$$

which can be bounded by using the Schwarz inequality. Hence

$$\frac{S}{N} \leq \sum_{j=0}^{2Bt} \frac{\alpha\{|s_j(j\Delta T)|^2\}^2 \Delta T}{|s_j(j\Delta T)|^2 + N_0' + \alpha(N_0'^2 + 2N_0'|s_j(j\Delta T)|^2)\Delta T} \tag{72}$$

which can again be recognized as the quantum limited condition.

4) Power Spectrum Analysis: In Section III it was shown that the time-averaged power density spectrum of the current could be written as

$$\bar{S}_i(\omega) = |H(\omega)|^2[E(N) + S_N(\omega)].$$

Since $S_N(\omega)$ is the spectrum of a nonnegative definite function (the normalized power), it can be written in terms of a dc and an ac component. The ac component is $S_{AC}(\omega)$ where

$$S_{AC}(\omega) = (\eta\bar{n}e)^2\Phi_M(\omega)$$

and $n(t)$ has been normalized to

$$n(t) = \bar{n}(1 + m(t)); \qquad m(t) \geq -1$$

with

$$\int_{-T}^{T} m(t)\,dt = 0$$

and $\Phi_M(\omega)$ the time-average power density spectrum of $m(t)$. Notice that the modulation index is included in $m(t)$. For an unmodulated source, such as noise, $m(t) \equiv 0$, and only the shot noise term and the dc remain. Thus if we have a signal plus additive noise impinging on the detector, where the average noise rate is designated $\bar{n}_n$, the power density spectrum minus the dc terms can be written as

$$S_T(\omega) = e^2|H(\omega)|^2[\eta(\bar{n}_n + \bar{n}) + (\eta\bar{n})^2\Phi_M(\omega)] + \frac{2kT}{R}$$

where we have also included the thermal noise contribution. If we define the signal-to-noise ratio as the ratio of the total signal power

$$\frac{(e\eta\bar{n})^2}{2\pi}\int_{2W'}\Phi_M(\omega)\,d\omega$$

over the bandwidth of the signal, divided by the total nonsignal power over the same bandwidth:

$$\frac{1}{2\pi}\int_{2W'}\left[e^2|H(\omega)|^2\eta(\bar{n} + \bar{n}_n) + \frac{2kT}{R}\right]d\omega$$

then, assuming that $|H(\omega)|^2$ is "flat" over the $2W'$ region of interest

$$\frac{S}{N} = \frac{(\eta\bar{n}e)^2\left\{\frac{1}{2\pi}\int\Phi_M(\omega)\,d\omega\right\}}{\left[e^2\eta(\bar{n} + \bar{n}_n) + \frac{2kT}{R}\right]2W} \leq \frac{(\eta\bar{n})}{\left[1 + \frac{\bar{n}_n}{\bar{n}} + \frac{2kT}{e^2R\eta\bar{n}}\right]2W} \tag{79}$$

where W is now the cyclic frequency. Notice again that if e is replaced by Ae and the shot noise term $2\eta A^2e^2\bar{n}W = 2\eta AeI_{DC}W > 4kTW$, the device will be again shot-noise limited. The term

$$\frac{\eta\bar{n}}{2W} = \frac{\eta P}{2h\nu W}$$

can again be recognized as being related to the quantum limited condition.

VI. Summary Remarks

We have tried to present in this paper a review of the basic concepts in optical communications viewed strictly from a classical point of view, in the absence of any channel effects. In this vein, we have viewed the received signal as an electromagnetic field and described its interaction with a photodetector. We then described some of the fundamental properties of the resulting current flow as seen by the communications engineer.

The treatment in this paper is not complete, since the study of this problem has not finished. Consequently, some portions have been given more emphasis than others, while some have been omitted entirely. For example, in the literature the topic of continuous estimation for shot noise processes has barely been touched [13]. The same is true for synchronization in a shot noise environment [31], although this will be fundamental to any sophisticated optical communications system.

What has been attempted, rather, was a presentation which answered the questions concerning the physical modelling of the system and a reduction to the terms most useful for analysis. Where such analysis had reached a level of conveying a reasonably complete understanding of an aspect of the problem, it was also presented. It is hoped that this paper is thorough enough to motivate additional research in this area.

References

[1] R. J. Glauber, "The quantum theory of optical coherence," *Phys. Rev.*, vol. 130, pp. 2529–2539, June 1963.

[2] ——, "Coherent and incoherent states of the radiation field," *Phys. Rev.*, vol. 131, September 1963.

[3] ——, "Optical coherence and photon statistics," in *Quantum Optics and Electronics*, C. de Witt, *et al.*, Eds. New York: Gordon and Breach, 1965, pp. 65–185.

[4] L. Mandel and E. Wolf, "Coherence properties of optical fields," *Rev. Mod. Phys.*, vol. 37, pp. 231–287, April 1965.

[5] J. R. Klauder and E. C. G. Sudarshan, *Fundamentals of Quantum Optics*. New York: W. A. Benjamin, Inc., 1968.

[6] G. J. Troup, *Optical Coherence Theory*. London, England: Methuen, 1967.

[7] W. H. Louisell, *Radiation and Noise in Quantum Electronics*. New York: McGraw-Hill, 1964.

[8] L. Mandel, E. C. G. Sudarshan, and E. Wolf, *Proc. Phys. Soc.*, vol. 84, 1964.

[9] E. Fermi, *Rev. Mod. Phys.*, vol. 4, 1932.

[10] V. Fano, *Amer. J. Phys.*, vol. 29, 1961.

[11] H. L. Van Trees, *Detection, Estimation, and Modulation Theory, Part I*. New York: Wiley, 1968.

[12] S. O. Rice, "Mathematical analysis of random noise," *Bell Syst. Tech. J.*, vol. 23, pp. 282–332, 1944.

[13] S. Karp and J. R. Clark, "Photon counting: a problem in classical noise theory," *IEEE Trans. Inform. Theory*, vol. IT-16, pp. 672–680, November 1970.

[14] D. Slepian and H. O. Pollak, "Prolate spheroidal wave function, Fourier analysis, and uncertainty, I," *Bell Syst. Tech. J.*, vol. 40, pp. 43–64, 1961.

[15] H. J. Landau and H. O. Pollak, "Prolate spheroidal wave functions, Fourier analysis and uncertainty, II," *Bell Syst. Tech. J.*, vol. 40, pp. 65–84, 1961.

[16] ——, "Prolate spheroidal wave functions, Fourier analysis and uncertainty, III," *Bell Syst. Tech. J.*, vol. 41, pp. 1295–1336, 1962.

[17] B. Reiffen and H. Sherman, "An optimum demodulator for Poisson processes: photon source detectors," *Proc. IEEE*, vol. 51, pp. 1316–1320, October 1963.

[18] K. Abend, "Optimum photon detection," *IEEE Trans. Inform. Theory* (Correspondence), vol. 12, pp. 64–65, January 1966.

Reprinted from the PROCEEDINGS OF THE IEEE
VOL. 58, NO. 12, DECEMBER, 1970
pp. 1964–1965

Approximations for Lognormally Fading Optical Signals

Abstract—A lognormally distributed random variable can be used to approximate accurately a noncentral chi-square random variable. This letter uses this result to approximate the photoelectron count distribution of a lognormally fading optical signal.

In a recent article [1] it was shown that one can accurately approximate a noncentral chi-square random variable with a lognormally distributed random variable. In this letter we show how this result can be used to approximate the photoelectron count distribution of a lognormally fading optical signal. We also discuss some other implications of this approximation with regard to the actual nature of the fading.

Slow Lognormal Fading

Let

$$r(t) = s(t)e^{\chi + j\phi}, \qquad t \in [0, T] \tag{1}$$

with $s(t)$ a finite-energy deterministic function and χ a Gaussian random variable. ϕ is usually taken to be a uniformly distributed variable [2], but it is irrelevant to our discussion. The energy of $r(t)$ in $[0, T]$ can be written as

$$E_r = \int_0^T |r(t)|^2 dt = E_s e^{2\chi} \tag{2}$$

where

$$E_s = \int_0^T |s(t)|^2 dt. \tag{3}$$

The Poisson (photoelectron count) distribution with mean E_r, conditioned on χ, is given by

$$p_{n|\chi}(N|\chi) = \frac{[\alpha E_s e^{2\chi}]^N}{N!} e^{-\alpha E_s e^{2\chi}} \tag{4}$$

where $\alpha = \eta / h\nu$, η is the quantum efficiency of the photodetector, ν is the frequency, and h is Planck's constant. Conservation of energy requirements dictate that the mean of χ be the negative of its variance, σ^2 [2]. Thus the random variable $y = \ln \alpha E_s + 2\chi$ is normal with mean a and variance b^2, where

$$a = \ln \alpha E_s - 2\sigma^2, \qquad b^2 = 4\sigma^2. \tag{5}$$

Then

$$z = \alpha E_s e^{2\chi} = e^y \tag{6}$$

is a lognormal random variable, and

$$M_z(u) = E(e^{uy}) = E(z^u) = e^{au + \frac{1}{2}b^2u^2}. \tag{7}$$

Now, let

$$a = \psi(m) - \ln m + \ln(1 - Z_0) + \frac{Z_0}{m} \tag{8}$$

$$b^2 = \psi'(m) \tag{9}$$

with $\psi(m)$ the digamma function, and m and Z_0 real parameters to be determined from a and b^2. Combining (7), (8), and (9), we get

$$M_z(u) = \exp\left[\left\{\psi(m) - \ln m + \ln(1 - Z_0) + \frac{Z_0}{m}\right\}u + \left\{\frac{\psi'(m)}{2}\right\}u^2\right]. \tag{10}$$

Using the approximation given by Ohta and Koizumi [1], $M_z(u)$ can be written

Manuscript received May 17, 1970.

Reprinted by permission from
IEEE TRANSACTIONS ON INFORMATION THEORY
Vol. IT-16, No. 6, November 1970

Photon Counting: A Problem in Classical Noise Theory

SHERMAN KARP, MEMBER, IEEE, AND JOHN R. CLARK, STUDENT MEMBER, IEEE

Abstract—**In this paper we formulate the general problem of determining the photoelectron "counting" distribution resulting from an electromagnetic field impinging on a quantum detector. Although the detector model used was derived quantum mechanically, our treatment is wholly classical and includes all results known to date. This combination is commonly referred to as the semiclassical approach. The emphasis, however, lies in directing the problem towards optical communication.**

The electromagnetic field is assumed to be the sum of a deterministic signal and a zero-mean narrow-band Gaussian random process, and is expanded in a Karhunen–Loève series of orthogonal functions. Several examples are given. It is shown that all the results obtainable can be written explicitly in terms of the noise covariance function. Particular attention is given to the case of a signal plus white Gaussian noise, both of which are band-limited to $\pm B$ Hz. Since the result is a fundamental one, to add some physical insight, we show four methods by which it can be obtained. Various limiting forms of this distribution are derived, including the necessary conditions for those commonly accepted. The likelihood functional is established and is shown to be the product of Laguerre polynomials. For the problem of continuous estimation, the Fisher information kernel is derived and an important limiting form is obtained. The maximum a posteriori (MAP) and maximum-likelihood (ML) estimation equations are also derived. In the latter case the results are also functions of Laguerre polynomials.

Manuscript received January 26, 1970; revised April 10, 1970.
S. Karp is with NASA Electronics Research Center, Cambridge, Mass. 02139.
J. R. Clark was with NASA Electronics Research Center, Cambridge, Mass. He is presently with the Research Laboratory of Electronics, Massachusetts Institute of Technology, Cambridge, Mass. 02139.

evaluated at $u = e^{i\nu} - 1$; thus, we can confine our attention to the random variable m_t.

It is convenient to expand $a(\tau)$ in a Karhunen–Loéve series on $[0, t]$ [16]:

$$a(\tau) = \sum_{i=1}^{\infty} a_i\phi_i(\tau) = \sum_i (s_i + n_i)\phi_i(\tau). \tag{12}$$

The equality, of course, is in the sense of "limit-in-the-mean." The coefficients are given by

$$n_i = (n, \phi_i) \tag{13}$$

$$s_i = (s, \phi_i) \tag{14}$$

where

$$(x, y) = \int_0^t x(\tau)y^*(\tau)\, d\tau \tag{15}$$

and the $\{\phi_i\}$ are eigenfunctions of the integral equation

$$\lambda_i\phi_i(u) = K_n\phi_i = \int_0^t K_n(u, v)\phi_i(v)\, dv. \tag{16}$$

Here $K_n(u, v) = E\{n(u)n^*(v)\}$ is the covariance kernel of the noise. The $\{\phi_i\}$ are normalized so that $(\phi_i, \phi_j) = \delta_{ij}$.

It is clear from the orthonormality of the eigenfunctions that m_t can be written

$$m_t = \alpha \sum_i |a_i|^2 = \alpha \sum_i |s_i + n_i|^2. \tag{17}$$

Notice that m_t is the energy in the process at time t. Since $n(\tau)$ is a zero-mean Gaussian random process, the $\{n_i\}$ are Gaussian random variables, with $E(n_i) = 0$ and $E(n_in_j^*) = \lambda_i\delta_{ij}$. This orthogonality depends critically upon choosing the basis to satisfy (16) uniquely. If, however, there is no noise ($n(\tau) = 0$), $a(t) = s(\tau)$ can be expanded in any complete orthonormal set $\{\psi_i\}$ on $[0, t]$, and (16) is irrelevant. For this case, with $c_i = (a, \psi_i)$, (1) can be written

$$\Pr\{N_t = k \mid [a(\tau); 0 < \tau \le t]\} = (k!)^{-1}[\sum_i \alpha |c_i|^2]^k \exp[-\sum_i \alpha |c_i|^2]. \tag{18}$$

Each coordinate axis in the space contributes an independent Poisson variate N_{ti},

$$\Pr\{N_{ti} = k_i \mid [a(\tau); 0 < \tau \le t]\} = \Pr\{N_{ti} = k_i \mid c_i\} = [\alpha |c_i|^2]^{k_i}e^{-\alpha|c_i|^2}/k_i! \tag{19}$$

where $N_t = \sum_i N_{ti}$ and $k = \sum_i k_i$ [17]. This is clearly independent of the particular basis chosen; only the $\{c_i\}$ change. Each axis always contributes an independent Poisson variate. In addition, since $\sum_i |c_i|^2$ is the energy of $a(\tau)$ in $[0, t]$, the conditional density of N_t is independent of the functional form of $a(\tau)$. If we choose $\{\psi_i\}$ to be the sinusoidal set on $[0, t]$, then $|c_i|^2$ represents the energy of $a(\tau)$ at the frequency of ψ_i. If $a(\tau) = \psi_j(\tau)$ for some j, then $k = k_j$ and (18) reduces to (19) with $i = j$.

For the more general case of nonzero noise, we observe that only one particular orthonormal set can be used as a basis for expanding $a(\tau)$, if we desire each axis in the space to contribute an independent variate to N_t. That basis, of course, must satisfy $K_n\phi = \lambda\phi$, (16). (The only exception is white Gaussian noise, for which (16) is satisfied by any complete orthonormal set; then each axis in the space contributes an independent, identically distributed random variable.)

For narrow-band Gaussian noise, we now show that the contribution from each axis is an independent Laguerre-distributed variate and, consequently, that N_t can always be represented as the sum of independent Laguerre random variables.

The real and imaginary parts of $n_i = (n, \phi_i)$ are independent, each with variance $\lambda_i/2$, thus, ([18] p. 196),

$$p_{|a_i|}(A) = \begin{cases} \dfrac{2A}{\lambda_i} \exp\left[-\dfrac{|s_i|^2 + A^2}{\lambda_i}\right] \cdot I_0\left(2\dfrac{|s_i|}{\lambda_i}A\right) & A \ge 0 \\ 0 & \text{elsewhere} \end{cases} \tag{20}$$

the so-called Ricean density, where I_0 is the zero-order modified Bessel function of the first kind. It follows that $|a_i|^2$ has the density function

$$p_{|a_i|^2}(A) = \begin{cases} \dfrac{1}{\lambda_i} \exp\left[-\dfrac{|s_i|^2 + A}{\lambda_i}\right] \cdot I_0\left(2\dfrac{|s_i|}{\lambda_i}A^{1/2}\right) & A \ge 0 \\ 0 & \text{elsewhere.} \end{cases} \tag{21}$$

Since the $\{a_i\}$ are independent, it follows that the $\{|a_i|^2\}$ are also independent. Thus, from (11) and (17) we see that

$$M_{m_t}(u) = \prod_i E\{e^{\alpha|a_i|^2u}\}. \tag{22}$$

Now, with x a real Gaussian variate, $E\{e^{x^2u}\}$ is given by ([19] p. 396)

$$E\{e^{x^2u}\} = \frac{\exp[(E^2(x)u)/[1 - 2\operatorname{var}(x)u]]}{[1 - 2\operatorname{var}(x)u]^{1/2}}, \quad \left(\operatorname{Re} u < \frac{1}{2\operatorname{var}(x)}\right). \tag{23}$$

Thus,

$$M_{m_t}(u) = \prod_i \frac{1}{1 - \alpha\lambda_iu} \exp\left[\frac{\alpha|s_i|^2u}{1 - \alpha\lambda_iu}\right], \quad \left[\operatorname{Re} u < \frac{1}{\alpha \max_i \lambda_i}\right] \tag{24}$$

and

$$M_{N_t}(j\nu) = \prod_i \left\{\frac{1}{1 - \alpha\lambda_i(e^{i\nu} - 1)} \cdot \exp\left[\frac{\alpha|s_i|^2(e^{i\nu} - 1)}{1 - \alpha\lambda_i(e^{i\nu} - 1)}\right]\right\}. \tag{25}$$

much easier to find by evaluating $M_{N_t}(jv)$ first, rather than by going directly to (9), (34), and (35). In the examples to follow, this is certainly the case.

Noise Only—$(s(\tau) \equiv 0)$

Integrated White Noise—$K_n(u, v) = \rho^2 \min(u, v)$: Although this example appears to be only of academic value, it is illustrative of a particularly simple means of obtaining $p_{N_t}(k)$. It is well known that the eigenvalues of (16) are ([19], p. 196)

$$\lambda_i = [4\rho^2 t^2/\pi^2(2i-1)^2] \qquad i = 1, 2, 3, \cdots. \tag{38}$$

Inserting this in (24) and using a tabulated product rule, we get ([21] eq. 1.4313)

$$M_{m_t}(u) = \sec(\rho t \sqrt{\alpha u}). \tag{39}$$

The coefficients in the Taylor series expansion of (39) are the moments $\{\mu_i\}$ of m_t; since ([21], eq. 1.4119)

$$\sec x = \sum_{k=0}^{\infty} [|E_{2k}|/(2k)!]x^{2k}, \qquad (x^2 < \pi^2/4) \tag{40}$$

we have

$$\mu_k = [k!/(2k)!]|E_{2k}|(\alpha\rho^2 t^2)^k \tag{41}$$

and the $\{E_i\}$ are the Euler numbers. Equation (9) now gives $p_{N_t}(k)$ directly:

$$p_{N_t}(k) = \sum_{n=0}^{\infty} \frac{(-1)^n}{(2k+2n)!}\binom{k+n}{n}|E_{2k+2n}|(\alpha\rho^2 t^2)^{k+n}. \tag{42}$$

Because of the simple form of $M_{m_t}(u)$, we can find the counting distribution without first having to compute the cumulants $\{\kappa_i\}$. The mean and variance of the counts work out to be

$$E(N_t) = (\alpha/2)\rho^2 t^2 \tag{43}$$

$$\text{var}(N_t) = (\alpha/2)\rho^2 t^2 + (\alpha^2/6)\rho^4 t^4. \tag{44}$$

First-Order Markov Noise—$K_n(u, v) = P \exp - \beta|u - v|$: Equation (24) becomes

$$M_{m_t}(u) = \prod_i [1/(1 - \alpha\lambda_i u)] \tag{45}$$

with λ_i a solution of a transcendental equation [9]. Equation (45) has been evaluated by an indirect technique [14] and is given by

$$M_{m_t}(u) = e^{\beta t}\left\{\cosh\left[\beta t\left(1 - \frac{2P\alpha}{\beta}u\right)\right] + \frac{1 - (P\alpha/\beta)u}{1 - (2P\alpha/\beta)u}\sinh\left[\beta t\left(1 - \frac{2P\alpha}{\beta}u\right)\right]\right\}^{-1}. \tag{46}$$

This does not easily yield a useful expression for $p_{N_t}(k)$; however, using the Leibnitz differentiation rule, Bédard [3] has obtained recurrence relations for the counting distribution and its factorial moments. For certain limiting cases, approximate counting distributions have been obtained [7].

The mean and variance of N_t are easily found to be

$$E(N_t) = \alpha P t \tag{47}$$

$$\text{var}(N_t) = \alpha P t + [(\alpha P)^2/2\beta^2][2\beta t + e^{-2\beta t} - 1]. \tag{48}$$

Band-limited White Gaussian Noise: Let $n(\tau)$ be a white Gaussian process, band-limited to $\pm B$ Hz, with two-sided spectral height N_0. Taking the first $2Bt + 1$ eigenvalues of (16) to be the same (N_0), and the rest to be zero ([19], p. 193), (24) becomes

$$M_{m_t}(u) = [1/(1 - \alpha N_0 u)]^{2Bt+1}, \tag{49}$$

that is,

$$M_{N_t}(jv) = [1 - \alpha N_0(e^{jv} - 1)]^{(-2Bt+1)}. \tag{50}$$

This can be recognized as the characteristic function of the negative binomial distribution [17]

$$p_{N_t}(k) = \binom{2Bt + k}{k}\left(\frac{1}{1 + \alpha N_0}\right)^{2Bt+1}\left(\frac{\alpha N_0}{1 + \alpha N_0}\right)^k. \tag{51}$$

If $2Bt \ll 1 (t \ll 1/2B)$, only one eigenvalue of (16) is significant, and (50) reduces to

$$M_{N_t}(jv) = [1 - \alpha N_0(e^{jv} - 1)]^{-1}. \tag{52}$$

In other words, the counting distribution is Bose–Einstein:

$$p_{N_t}(k) = [1/(1 + \alpha N_0)][\alpha N_0/(1 + \alpha N_0)]^k \tag{53}$$

in agreement with (27). For $2Bt \gg 1$, and $\alpha N_0 \ll 1$, it can easily be shown that $p_{N_t}(k)$ approaches a Poisson distribution. (*Note:* This limiting form can also be shown to be true for first-order Markov noise, (46), when $\beta t \gg 1$ and $\beta \gg 4P\alpha$.) On the other hand, for a nonzero signal and no noise, $p_{N_t}(k)$ is also Poisson, as we have seen. This behavior, in the case of band-limited white Gaussian noise, is due to the complete "smoothing out" of the intensity fluctuations, while in the signal-only case, it is due to the deterministic nature of the signal.

Signal Plus Noise

Now we remove the restriction that $s(\tau)$ be zero. Assume that $n(\tau)$ is band-limited white Gaussian noise, as above. In addition, assume that $s(\tau)$ is band-limited to $\pm B'$ Hz, $B' \leq B$. Equation (25) applies with $\lambda_i = N_0$, and $p_{N_t}(k)$ is just the $(2Bt + 1)$-fold convolution of the Laguerre density (26) with itself. Omitting the details, we note that the result is ([21], eq. 8.9771)

$$p_{N_t}(k) = \frac{(\alpha N_0)^k}{(1 + \alpha N_0)^{k+2Bt+1}} \cdot \exp\left[-\frac{\alpha(s, s)}{1 + \alpha N_0}\right] L_k^{2Bt}\left[\frac{-(s, s)}{N_0(1 + \alpha N_0)}\right] \tag{54}$$

where L_k^{2Bt} is the $2Bt$-order Laguerre polynomial. The mean and variance of N_t are found to be

$$E(N_t) = (2Bt + 1)\alpha N_0 + \alpha(s, s) \tag{55}$$

$$\text{var}(N_t) = (2Bt + 1)(1 + \alpha N_0)\alpha N_0 + (1 + 2\alpha N_0)\alpha(s, s). \tag{56}$$

$$c(k_i, s_i) = \frac{1}{\alpha N_0} \frac{L^1_{k_i-1}\{-(|s_i|^2)/[N_0(1+\alpha N_0)]\}}{L_{k_i}\{-(|s_i|^2)/[N_0(1+\alpha N_0)]\}} - 1. \quad (70)$$

The problem is now simplified if we consider x as a set of parameters (say, M of them). Then, with $x = (x_1, x_2, \cdots, x_M)$, (69) reduces to the set of M expressions:

$$\nabla_x \ln \Lambda = \frac{2\alpha}{1+\alpha N_0} \sum_{i=1}^{2Bt} c(k_i, s_i) \operatorname{Re}\left[s_i^* \frac{\partial s_i}{\partial x_k}\right]$$
$$k = 1, 2, \cdots, M. \quad (71)$$

Further simplication is possible if s is a memoryless mapping; thus, with $x_i = x(i/2B)$, (69) becomes

$$\nabla_x \ln \Lambda = \frac{2\alpha}{1+\alpha N_0} c(k_i, s_i) \operatorname{Re}\left[s_i^* \frac{\partial s_i}{\partial x_i}\right]$$
$$i = 1, 2, \cdots, 2Bt. \quad (72)$$

In general, it appears that a search procedure is necessary to find $\hat{x}_{MAP}$ or $\hat{x}_{ML}$.

If we now assume that the a priori density $p_{x(\tau)}[x(\tau)]$ is Gaussian, then (67) reduces to

$$\dot{\hat{x}}(\tau) = \frac{2\alpha}{(1+\alpha N_0)} \sum_{i=1}^{2Bt} \left\{\frac{(1/\alpha N_0) L^1_{k_i-1}\{-(|s_i|^2)/[N_0(1+\alpha N_0)]\}}{L_{k_i}\{-(|s_i|^2)/[N_0(1+\alpha N_0)]\}} - 1\right\} \operatorname{Re}\left[s_i^* \frac{\partial s_i}{\partial x(\tau)}\right]\Bigg|_{x(\tau)=\hat{x}(\tau)} \quad (0 < \tau \le t) \quad (73)$$

which, as we can see from Fig. 1, has very limited use. However, by making one more assumption, namely, that the average noise count per degree of freedom is small:

$$\alpha N_0 \ll \min[\alpha|s_i|^2, 1] \quad (74)$$

(73) reduces to

$$\dot{\hat{x}}(\tau) \cong \sum_{i=1}^{2Bt} [k_i - \alpha |s_i|^2] \frac{\partial}{\partial x(\tau)} \ln |s_i|^2 \Big|_{x=\hat{x}(\tau)} \quad 0 < \tau \le t \quad (75)$$

and is shown in Fig. 2.

Notice that the optimum MAP estimate is performed on the intensity of the process. That is, k_i is first compared to $\alpha|s_i|^2$, the expected count of the received process. Since $|s_i|$ is the envelope of the process, it can be written as $e^{\ln|s_i|}$, and $(\partial/\partial\hat{x}) \ln |s_i|$ serves the same function as $(\partial/\partial\hat{x})s(t, x)$ in the MAP equations for Gaussian systems ([19] p. 432).

If the intensity of the process is constant, such as FM, no phase information can be obtained since $(\partial/\partial x) \ln |s_i| = 0$, making $\dot{\hat{x}} = 0$. To obtain phase information from an FM or a PM signal, optimal heterodyne detection must be employed. That is, the signal from a local oscillator is aligned and mixed with the received signal over the surface of the detector. Then,

$$s_i = E_1 e^{j\omega_1 t + \phi(t)} + E_{L_0} e^{j\omega_0 t}$$

where E_1 and E_{L_0} are the two electric field strengths, and

$$|s_i|^2 = |E_1|^2 + |E_{L_0}|^2 + \{E_1 E^*_{L_0} e^{j[(\omega_1-\omega_0)t+\phi]} + E^*_1 E_{L_0} e^{-j[(\omega_1-\omega_0)t+\phi]}\}. \quad (76)$$

Assuming narrow-band signals, we have

$$|s_i|^2 \simeq |E_1|^2 + |E_{L_0}|^2 + 2E_1 E_{L_0} \cos[(\omega_1 - \omega_2)t + \phi(t)]. \quad (77)$$

By making the local oscillator signal large $|E_{L_0}| \gg |E_1|$,

$$|s_i|^2 \simeq |E_{L_0}|^2 \left\{1 + \frac{2E_1}{E_{L_0}} \cos[(\omega_1 - \omega_2)t + \phi(t)]\right\} \quad (78)$$

and

$$\ln |s_i| = \tfrac{1}{2} \ln |s_i|^2 \simeq \ln |E_{L_0}| + \frac{E_1}{E_{L_0}} \cos[(\omega_1 - \omega_2)t + \phi(t)].$$

Hence,

$$\frac{\partial}{\partial x(\tau)} \ln |s_i| \simeq -\frac{E_1}{E_{L_0}} \frac{\partial \phi}{\partial x(\tau)} \sin[(\omega_1 - \omega_2)t + \phi(t)]. \quad (79)$$

We see, then, that the optimum detector is similar, in this case, to a phase-lock loop. It can also be shown by using (26) and [18] and [26] that if we consider the random variable k_i as a shot-noise process and pass it through a narrow-band filter with bandwidth 2ω tuned to $(\omega_1 - \omega_2)$, the density will approach a Gaussian density with mean $2\alpha E_1 E_{L_0} \cos[(\omega_1 - \omega_2)t + \phi(t)]$ and variance $\alpha|E_{L_0}|2W$.

Using the notion of an *information kernel*, we can lower-bound the mean-square error of *any* estimator resulting from (66), without specifying the form of the estimator ([19] p. 80). Defining

$$J_D = E\left[\frac{\partial \ln \Lambda}{\partial x(u)} \frac{\partial \ln \Lambda}{\partial x(v)}\right] \quad (80)$$

$$J_P = E\left[\frac{\partial \ln p_{x(\tau)}[X(\tau)]}{\partial x(u)} \frac{\partial \ln p_{x(\tau)}[X(\tau)]}{\partial x(v)}\right] \quad (81)$$

$$J_T = J_D + J_P = \text{information kernel} \quad (82)$$

we can show that

$$\int_0^t [x(\tau) - \hat{x}(\tau)]^2 \, d\tau \ge \operatorname{Tr} J_T^{-1}. \quad (83)$$

The expectation in (80) and (81) is over the random function x. Combining (69) and (80), we have

$$J_D = E\left\{\frac{4\alpha^2}{(1+\alpha N_0)^2} \sum_{i=1}^{2Bt} \sum_{j=1}^{2Bt} c(k_i, s_i) \cdot c(k_j, s_j) \operatorname{Re}\left[s_i^* \frac{\partial s_i}{\partial x(u)}\right] \operatorname{Re}\left[s_j^* \frac{\partial s_j}{\partial x(v)}\right]\right\}. \quad (84)$$

To evaluate this further, the transformation s must be specified.

Conclusions

We have presented general results for the photoelectron counting distributions arising from the quantum detection of a narrow-band Gaussian process. The semiclassical approach has led to probability distributions that could

of Quantum Electronics, P. L. Kelly *et al.*, Eds. New York: McGraw-Hill, 1965, pp. 788–811.
[7] C. W. Helstrom, "The distribution of photoelectric counts from partially polarized Gaussian light," *Proc. Phys. Soc.*, vol. 83, pp. 777–782, 1964.
[8] J. Peřina, "Determination of the statistical properties of light from photoelectric measurements," *Czech J. Phys.*, vol. B17, p. 1086, 1967.
[9] D. Middleton, *Introduction to Statistical Communication Theory*. New York: McGraw-Hill, 1960.
[10] R. C. Emerson, "First probability densities for receivers with square-law detectors," *J. Appl. Phys.*, vol. 24, p. 1168, 1953.
[11] D. Slepian, "Fluctuations of random noise power," *Bell Sys. Tech. J.*, vol. 37, pp. 163–184, 1958.
[12] M. Kac and A. J. F. Siegert, "On the theory of noise in radio receivers with square-law detectors," *J. Appl. Phys.*, vol. 18, p. 383, 1947.
[13] D. A. Darling and A. J. F. Siegert, "A systematic approach to a class of problems in the theory of noise and other random phenomena: Pt. I," *IRE Trans. Information Theory*, vol. IT-3, pp. 32–36, March 1957.
[14] A. J. F. Siegert, "A systematic approach to a class of problems in the theory of noise and other random phenomena: Pt. II—Examples," *IRE Trans. Information Theory*, vol. IT-3, pp. 38–43, March 1957.
[15] M. Ohta and T. Koizumi, "Intensity fluctuation of stationary random noise containing an arbitrary signal wave," *Proc. IEEE* (Letters), vol. 57, pp. 1231–1232, June 1969.
[16] W. Davenport and W. L. Root, *Introduction to Random Signals and Noise*. New York: McGraw-Hill, 1958.
[17] E. Parzen, *Stochastic Processes*. San Francisco, Calif.: Holden-Day, 1962.
[18] A. Papoulis, *Probability, Random Variables, and Stochastic Processes*. New York: McGraw-Hill, 1965.
[19] H. L. Van Trees, *Detection, Estimation, and Modulation Theory, Part I*. New York: Wiley, 1968.
[20] G. Lachs, "Theoretical aspects of mixtures of thermal and coherent radiation," *Phys. Rev.*, vol. 138, pp. B1012–B1016, 1965.
[21] I. S. Gradshteyn and I. M. Ryzhik, *Table of Integrals Series and Products*. New York: Academic Press, 1965.
[22] R. Deutsch, *Nonlinear Transformations of Random Processes*. Englewood Cliffs, N. J.: Prentice-Hall, 1962.
[23] R. Courant and D. Hilbert, *Methods of Mathematical Physics*, vol. 1. New York: Interscience, 1953.
[24] M. G. Kendall and A. Stuart, *The Advanced Theory of Statistics*, vol. 1. London: Griffin, 1963.
[25] J. R. Klauder and E. C. G. Sudarshan, *Fundamentals of Quantum Optics*. New York: Benjamin, 1968.
[26] S. Karp, "A statistical model for radiation with applications to optical communications," Ph.D. dissertation, Dept. of Elec. Engrg., University of Southern California, Los Angeles, 1967.
[27] J. W. S. Liu, "Reliability of quantum-mechanical communication systems," M.I.T. Research Lab. of Electron., Cambridge, Mass., Tech. Rept. 468, December 31, 1968.
[28] G. L. Fillmore and G. Lachs, "Information rates for photocount detection systems," *IEEE Trans. Information Theory*, vol. IT-15, pp. 465–468, July 1969.
[29] B. Reiffen and H. Sherman, "An optimum demodulator for Poisson processes: Photon source detectors," *Proc. IEEE*, vol. 51, pp. 1316–1320, October 1963.
[30] R. M. Gagliardi and S. Karp, "*M*-ary Poisson detection and optical communications," *IEEE Trans. Communications Technology*, vol. COM-17, pp. 208–216, April 1969.